HHS Public Access

Author manuscript

Chem Rev. Author manuscript; available in PMC 2019 February 01.

Published in final edited form as:

Chem Rev. 2017 February 22; 117(4): 2711–2729. doi:10.1021/acs.chemrev.6b00400.

Fighting Cancer with Corroles

Ruijie D. Teo[†], **Jae Youn Hwang**[‡], **John Termini**[*,§], **Zeev Gross**[*,⊥], and **Harry B. Gray**[*,†]

[†]Division of Chemistry and Chemical Engineering, California Institute of Technology, Pasadena, California 91125, United States

[‡]Department of Information and Communication Engineering, Daegu Gyeongbuk Institute of Science & Technology, Daegu, Republic of Korea.

[§]Department of Molecular Medicine, Beckman Research Institute of the City of Hope, 1500 E. Duarte Road, Duarte, California 91010, United States

[⊥]Schulich Faculty of Chemistry, Technion—Israel Institute of Technology, Haifa 32000, Israel

Abstract

Corroles are exceptionally promising platforms for the development of agents for simultaneous cancer-targeting imaging and therapy. Depending on the element chelated by the corrole, these theranostic agents may be tuned primarily for diagnostic or therapeutic function. Versatile synthetic methodologies allow for the preparation of amphipolar derivatives, which form stable noncovalent conjugates with targeting biomolecules. These conjugates can be engineered for imaging, targeting, as well as therapeutic function within one theranostic assembly. In this review, we begin with a brief outline of corrole chemistry that has been uniquely useful in designing corrole-based anticancer agents. Then we turn attention to the early literature regarding corrole anticancer activity, which commenced one year after the first scalable synthesis was reported (1999–2000). In 2001, a major advance was made with the introduction of negatively charged corroles, as these molecules, being amphipolar, form stable conjugates with many proteins. More recently, both cellular uptake and intracellular trafficking of metallocorroles have been documented in experimental investigations employing advanced optical spectroscopic as well as magnetic resonance imaging techniques. Key results from work on both cellular and animal models are reviewed, with emphasis on those that have shed new light on the mechanisms associated with anticancer activity. In closing, we predict a very bright future for corrole anticancer research, as it is experiencing exponential growth, taking full advantage of recently developed imaging and therapeutic modalities.

Graphical Abstract

[*]**Corresponding Authors** jtermini@coh.org. [*] chr10zg@tx.technion.ac.il. [*] hbgray@caltech.edu.

Notes

The authors declare no competing financial interests.

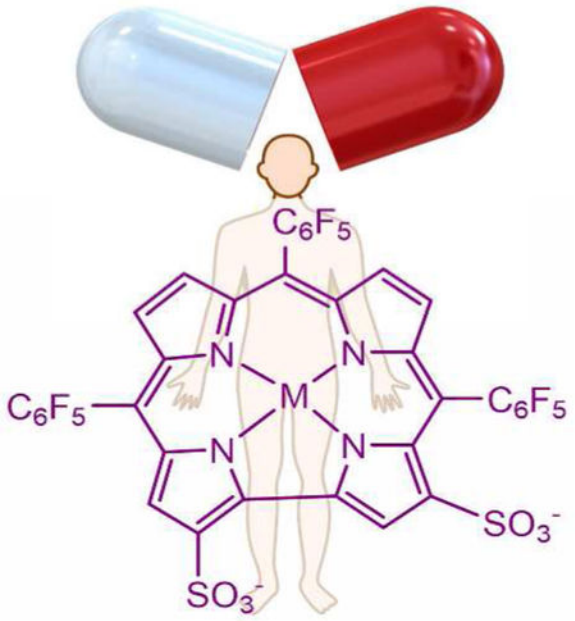

1. Introduction

Cancer has been an intractable disease since the beginning of recorded time. It was first documented in an Egyptian textbook dated about 3000 B.C., in which the writer declared that: “There is no treatment.”[1] Today, in spite of dramatic advances in biology and medicine, cancer incidence continues to increase and has reached epidemic proportions; it is projected to increase from 14 million annual cases documented in 2012 to 22 million within the next two decades.[2] Lung and breast cancers are most common in men and women.[3] Before the advent of modern medicine, tumors were treated crudely by excisions with knives, burning with red-hot irons, fumigations, topical applications of pastes, spells and advice to leave the swelling untreated.[4] Today, successful treatments of cancer have emerged – surgery, radiation therapy, chemotherapy, immunotherapy, targeted therapy, hormone therapy, and stem cell transplants.[5] In recent times, chemotherapy using cytotoxic agents that affect both normal and cancerous cells has been a standard approach.[6] More targeted therapy employing cytotoxic and/or cytostatic drugs that inhibit tumor cells specifically is becoming the preferred treatment of choice.[7] From a chemist’s perspective, it would be highly beneficial to improve both the specificity and efficacy of targeted chemotherapy through development of new classes of cytotoxic and cytostatic small molecules. In this regard many promising avenues remain less than fully explored, including the myriad opportunities provided by metal ion containing drugs. Inorganic drugs are not new: Egyptians used selenium-containing garlic as early as 1550 B.C. to treat a wide variety of ailments.[8] In the 20th century, a platinum compound, *cis*-dichlorodiammineplatinum(II), or cisplatin, was introduced. Called the penicillin of anticancer drugs, it has saved the lives of countless cancer patients. The 1979 approval of cisplatin as an anticancer drug by the Food and Drug Administration (FDA)[9] greatly energized investigators of metal-containing drugs (metallodrugs).[10] An ongoing search for improved platinum-based drugs – driven in part because of cisplatin resistance –has resulted in FDA approval of two other complexes for

cancer treatment: carboplatin[11] and oxaliplatin.[12] Contemporary research in this field[13,14] is focused on both platinum(II) and platinum(IV) complexes, as well as on molecular agents containing gold,[15] ruthenium,[16] iridium,[17] and a few other transition metals.[18] It is encouraging that many metal complexes are now under development for treatment of cancer and other diseases.[19–21]

Another “small-molecule approach” for cancer treatment is photodynamic therapy (PDT), which relies on photosensitizers that accumulate selectively in tumors and induce cytotoxicity via the generation of singlet oxygen or reactive oxygen species (ROS) upon irradiation by (preferably) tissue-penetrating wavelengths of visible light.[22] The basic concept has been known for many decades and the most promising drug candidates are based on oligopyrrolic macrocycles such as porphyrins and phthalocyanines.[23,24] The earliest FDA approved drug from that family of compounds was Photofrin®,[25] which is quite surprising considering that it is actually a mixture of many porphyrins. Also approved was 5-aminolaevulinic acid (ALA, traded as Levulan®),[26] the biosynthetic precursor of all natural oligopyrrolic macrocycles (heme, chlorophyll, Vitamin B12, and more).[27] On the other hand, only very few synthetic or semisynthetic porphyrinoid derivatives are in current clinical use.[28] One prominent example is the aluminum complex of bis-sulfonated phthalocyanine.[29] Although investigative work aimed at drug approval revealed that this compound is a very effective PDT agent acting via *necrosis*, one issue could not be resolved: the “compound” is actually a mixture of at least 16 isomers that could not be separated.[30] Many other examples of cytotoxic and phototoxic metalloporphyrin derivatives have been reported, ranging from ruthenium-based “extended-arms” porphyrins[31] to tetraarylporphyrin-platinum conjugates.[32] It is quite surprising, however, that very little is known about the systemic toxicities of the parent metal complexes (metalloporphyrins).[33–34] One likely explanation is that many of them undergo demetallation under biological conditions.[35–36]

There has been a great deal of work on expanded porphyrins,[37–39] and some derivatives have reached advanced clinical stages of clinical testing.[40] Much less information is available for contracted porphyrins, macromolecular entities that include corroles as major players. Corroles were first introduced in the 1960s (owing in part to the interest in vitamin B_{12}),[41] but research on these molecules and their metal derivatives did not flourish primarily because scalable methods for their preparation were not available.[42] This obstacle was removed near the end of the last century with the disclosure of the first facile synthesis of a corrole that was stable in its free-base form, H_3(tpfc), via condensation of pyrrole and the appropriate aldehyde.[43] It was this breakthrough that propelled research on corroles (Figure 1), resulting in developments that ranged from fundamental coordination chemistry of the corresponding metal complexes (metallocorroles) to practical applications in chemistry and biology. One highlight was the introduction of metallocorroles for prevention (and treatment) of oxidative stress-induced diseases (cardiovascular, neurodegenerative, and diabetes), as well as cancer theranostics. We will review work in the latter area with emphasis on the promise of metallocorroles for the diagnosis and treatment of cancer.

2. Corrole Properties of Relevance to Cancer Treatment

2.1 Metallation, Demetallation, and Formal Oxidation States

While the “periodic table of corroles” is still less extensive than that of porphyrins, the knowledge that has accumulated during the last two decades has revealed a variety of unambiguous trends, of which several are very important regarding the utility as metallodrugs. The insertion of transition and post-transition elements into the N4 coordination core of corroles affords complexes in which the formal oxidation state of the metal is +3 or higher, irrespective of the oxidation state of the metal precursor. This property may be attributed to the macrocyclic corrole framework acting as a trianionic ligand, rather than dianionic as in porphyrins or monanionic as in corrin, the cobalt-chelator in vitamin B12. Less obvious is that the metal-nitrogen bonds in metallocorroles are much more covalent than those in analogous metalloporphyrins.[44–45] One important consequence of enhanced covalency is that metallocorroles are stable toward hydrolysis,[46] and not prone to metal ion loss under physiologically relevant conditions.[47] The combination of σ metal-ligand covalency and π-electron noninnocence means that metal oxidation states are hard to assign in many cases. It follows that the oxidation states adopted in this review must be viewed as “formal” ones in which the chelating corrole is assumed to be a trianionic closed-shell ligand. Such oxidation state designations are useful, as transition metal corroles are less oxidizing than analogous porphyrins for any given formal oxidation state, a property of relevance in discussions of anticancer activities.

2.2 Photophysical Properties

The most striking photophysical property of a metallocorrole is intense fluorescence compared to that of closely related macromolecules. While the quantum yield of tetraphenylporphyrin (H_2TPP) is reduced from 0.11 to 0.033 upon zinc(II) insertion and only slightly increased (0.165) in its magnesium(II) derivative,[48] it is enhanced from 0.17 in 5,10,15-tris(pentafluorophenyl)corrole (H_3(tpfc)) to 0.37 and 0.76 in the corresponding gallium(III) and aluminum(III) complexes, Ga(tpfc)(py)[49] and Al(tpfc)$(py)_2$, respectively (Chart 1).[50–51] The early work was followed by many articles that looked deeper into the photophysical properties of a variety of corroles and their metal complexes.[52–54] Notably, phosphorous corroles have enjoyed recent attention[55–56] because of their use in the photodynamic inactivation of biofilms and bacteria.[57]

2.3 Amphipolar Corroles

Insertion of heavy metal ions along with facile and selective functionalization of the macrocyclic framework have been employed successfully for tuning the spectroscopic, chemical, biological and physical properties of corroles for imaging and therapeutic applications.[58–59] Insertion of Ir(III)[60] and Au(III)[61] affords complexes that display phosphorescence at room temperature; interestingly, the same may be achieved by introducing other heavy atoms (mainly iodine) on the corrole skeleton. The heavy atom effect also may be exploited for singlet oxygen generation by photosensitization with metallocorroles, an effect most pronounced for Sb(III) substituted analogues.[62] While simple triarylcorroles are lipophilic and insoluble in water, derivatives with polar and/or ionic residues have facilitated biological applications. The introduction of polar functionality

can be accomplished in a manner analogous to that previously demonstrated for porphyrins; however, the extreme electron density afforded by the two directly connected pyrrole rings in corroles allows for different approaches for functionalization. The most commonly employed method is the highly selective double chlorosulfonation of H_3(tpfc), which after hydrolysis affords **1**-H_3 (Chart 2). This corrole and its metal complexes **1**-M are amphipolar, resembling natural heme by virtue of two negative charges located on one pole of the otherwise lipophilic molecule. This amphipolarity accounts for the observation that **1**-Ga and heme bind to the same subdomain of albumin,[63–64] as well as for the high affinity of the various **1**-M complexes for many other proteins, including the cholesterol carrying low-density lipoprotein (LDL) and high-density lipoprotein (HDL).[65]

3. Positively Charged Corroles as Anticancer Agents

The publication of the first facile synthesis of a stable free-base corrole also described the synthesis of the first water soluble corrole, P1021 (Chart 3). The earliest report of corroles as anticancer agents was published soon after, including P1021 in a study that focused primarily on the synthesis of porphyrins with positively charged substituents (Chart 3).[66]

The most promising porphyrin based on *in vitro* studies was P1016, which carries positive charges on three out of the four meso-C atoms of the macrocycle. The synthesis of such porphyrin derivatives is very challenging, while it is much more feasible for corroles, simply because they have only three *meso*-C atoms. Comparison of the compounds depicted in Chart 1 in a mouse model of human lung cancer revealed that P1021 corrole was the most potent inhibitor of lung metastasis, as illustrated by the data in Figure 2. P1021 was found to be about 10-fold more active than TMPP *in vitro* and 5-fold more potent in an *in vivo* tumor model, inhibiting lung metastasis in mice at a concentration of only 5 mg/kg body weight.[66]

Work on corrole P1021 was not continued, because its synthesis required the use of n-butyllithium and very precise control of low temperature reaction conditions, which likely would render impractical any large-scale synthetic effort for pharmacological testing. However, simpler corroles that also are water soluble owing to positively charged substituents have been studied in greater detail (Chart 4).[67–74]

The first indication that corrole metal complexes might have anticancer activity came from work on **2**-Mn (Chart 4), which was found to intercalate DNA more strongly than the analogous porphyrin **3**-Mn.[67] It was suggested that porphyrin binding is restricted to the major and minor grooves of DNA, owing to the requirement of at least one strongly bound anionic axial ligand that would tend to preclude intercalation. However, manganese(III) corroles are neutral and form only 5-coordinate complexes with rather weakly bound neutral axial ligands.[75] It has also been shown that metal-free corroles **4**-H_3 and **5**-H_3 stabilize G-quadruplex DNA, a distinguishing feature of chromosome telomeres, suggesting a potential application as telomerase inhibitors.[68] The authors attributed the affinity for quadruplex DNA to the planar arrangement of corrole rings that facilitated pi-stacking with base pairs along with the appropriate disposition of positively charged functional groups that contributed electrostatic stabilization via interaction with the negatively charged phosphate backbone.[68] Inhibition of telomerase activity was tested, revealing IC_{50} values of 8.6 and 4.4

μM for **4**-H_3 and **5**-H_3, respectively. Subsequent investigation showed that out of the eight cationic corroles comprising the manganese (**4**-Mn) and copper derivatives (**6**-Cu −**11**-Cu), **4**-Mn stabilized telomeric G-quadruplex sequences 21G and Pu27 at very low concentrations.[69] It has been suggested that this feature of **4**-Mn may be attributed to the electron-withdrawing pyridinium moiety, which by decreasing electron density in the corrole ring leads to stronger interactions with the more electron-rich G-quaduplex DNA.[76,77] A more recent paper reported that **4**-e(OH) can distinguish single-stranded (ss) polyadenylic and polycytidylic acids, while **4**-H_3 can discriminate between ss and double-stranded (ds) conformations of nucleic acid homopolymers, preferentially binding to ss DNA.[77]

In light of their selective modes of DNA binding, some of these derivatives were examined as potential new anticancer agents.[78,79] **13**-Mn was found to be cytostatic and cytotoxic against breast, ovarian, and melonoma cell lines, while **12**-Mn was neither cytostatic nor cytotoxic against the same panel at the concentrations studied (up to 30 μM).[71] The lack of anticancer activity of **12**-Mn was attributed to the presence of *ortho*-alkyl groups, which prevented DNA intercalation.

Interestingly, the cytotoxicity of **4**-Ga against Hep G2 cells increased by 3 orders of magnitude, from an IC_{50} value of > 80 μM in the dark to 0.06 μM when deployed as a photodynamic agent.[74] Flow cytometry studies showed that the apoptotic population (sub-G_0 phase) of Hep G2 cells increased to 46% when treated with 0.06 μM **4**-Ga under red light irradiation. The photocytotoxicity of **4**-Ga was attributed to irradiation-induced apoptosis, while ultraviolet−visible (UV-vis) titrations, circular dichroism, polymerase chain reaction stop assays, and molecular docking studies suggested that c-Myc G-quadruplex DNA was stabilized by **4**-Ga, suggesting potential inhibition of telomerase activity.

Although these results are encouraging, it is not yet known how effective cationic metallocorroles will be as anticancer therapeutics, as experimental work with appropriate animal models has not yet been reported. More data are currently available on the utility of positively charged manganese(III) porphyrins for *the prevention of* oxidative damage by catalytic decomposition of ROS and reactive nitrogen species (RNS), which can also contribute to their anticancer activity.[80] A study[72] that focused on protection against both H_2O_2-and linsidomine-induced cytotoxicity in mouse motor neuron-neuroblastoma fusion NSC-34 cell lines demonstrated that **2**-Mn and **12**-Mn were very effective against damage attributable to *intracellular* peroxynitrite (Chart 4).[81–83] In the same study, the administration of positively charged **2**-Mn at 20 μM almost completely abolished linsidomine-induced tyrosine nitration, while treatment with **1**-Mn led only to partial reduction.[72] Here it is important to point out that increased levels of ROS have been implicated in carcinogenesis;[84–86] and that manipulating ROS levels by redox modulation is a way to kill cancer cells selectively without causing significant toxicity to normal cells.[87] As ROS signalling contributes to proliferation and survival in many cancers, the ability of corroles to rescue and disrupt mitochondria redox communication could potentially be exploited in cancer therapeutic interventions.[88–91]

4. Negatively Charged Amphipolar Corroles

4.1 Corrole/Protein Interactions and Cellular Uptake

The most thoroughly investigated corrole for therapeutic applications contains two sulfonic acid head groups on two adjacent and directly bound pyrroles of the macrocyclic skeleton (2,17-bis-sulfonato-5,10,15-trispentafluorophenylcorrole**, 1**-H_3, Chart 2).[92] This corrole and its metal derivatives **1**-M (also shown in Chart 2) are amphipolar: they possess hydrophilic sulfonic acid moieties on only one pole of the otherwise hydrophobic molecule. As the sulfonic acid head groups are fully ionized at physiological pH, cellular uptake and internalization might be disfavored, since cell membranes also are negatively charged. That cellular uptake is not diminished has been documented in many studies, including one that compared the uptake of **1**-Fe and Fe(TPPS), a water soluble iron(III) porphyrin that is not amphipolar, as it has four symmetrically distributed sulfonic acid head groups. The intracellular concentration of **1**-Fe in macrophages was found to be much greater, which was attributed to its interaction with amphipolar proteins that facilitated cellular uptake.[93] This finding was reminiscent of earlier work which showed that **1**-a undergoes endocytosis by breast cancer cells with the participation of various proteins, including serum albumin. The most direct evidence for assisted uptake came from work demonstrating that lipofectin (a transfection reagent) and an adenovirus serotype 5 (Ad5) capsid penton base function as carrier molecules for **1**-H_3.[59] In protein-free media, the corrole appeared to aggregate at the cell surface (Figures 3a–c), while enhanced intracellular corrole fluorescence was observed in the presence of penton base (Figures 3d–f) or lipofectin (Figures 3g–i), confirming assisted cellular uptake of these corroles.

The above work was followed by investigations that focused on the spontaneous bio-conjugation of corroles with albumin[63] and transferrin.[94] Albumin was chosen because of accumulating evidence that drug/albumin conjugates are promising formulations for targeting cancer.[95] Fluorescence quenching experiments exploiting the unique tryptophan present in human serum albumin (HSA) in conjunction with molecular modeling led to the identification of plausible binding sites for **1**-Ga (Figure 4). In related work, transferrin was identified as a potential targeting vehicle for corroles due to its affinity for endothelial cells associated with the blood-brain barrier.[96] Although corrole binding to both HSA and transferrin was very strong ($K_d \leq 1$ nM and 10 nM, respectively), it was shown that transferrin-based targeting may not be practical, since the protein is much less abundant *in vivo* than HSA and **1**-H_3 pre-bound to transferrin is rapidly redistributed to HSA even under equimolar conditions.[94]. This result indicated that pre-complexation of corroles with carrier proteins may lead to redistribution even under conditions where there should be no free corrole in solution according to the K_d values obtained from work on isolated proteins. Later studies hence focused on the distribution of **1**-H_3 and its metal complexes in whole serum, which revealed remarkable binding preferences for LDL (15%) and HDL (85%) relative to all other available proteins.[65,97] These results suggest that lipoproteins may act as primary carriers during circulation of corroles, including ones conjugated to smaller proteins that have targeting properties. Indeed, very selective corrole delivery was achieved employing the semisynthetic protein described below.

In parallel with the aforementioned binding studies of **1**-H_3 and **1**-M with serum proteins, work was performed aimed at conjugating corroles with specific receptor-targeting proteins capable of penetrating cells. In 2006, the gallium(III) complex of the sulfonated corrole, **1**-Ga (Chart 2) was shown to form a non-covalent conjugate with a heregulin-targeted adenovirus penton fusion protein HerPBK10 (Scheme 1).[59] Examination by several independent methodologies revealed that pre-incubation of **1**-a with HerPBK10 led to a very tight bioconjugate, termed HerGa, which did not exchange its bound corrole with serum proteins.[98] The motivation for conjugating the corrole with HerPBK10 was that the latter specifically binds to ErbB receptors that are prevalent on the cell surface of ErbB2+ human breast cancer cells,[99,100] including MDA-MB-435 and MDA-MB-453 cell lines, thereby allowing for receptor-mediated cell entry. Furthermore, as a derivative of the Ad5 capsid penton base protein,[101,102] HerPBK10 can undergo endosomolysis and subsequent translocation into the cytosol.[103] *In vivo* imaging experiments exploiting the intense fluorescence of **1**-Ga strongly suggested that HerGa retains HerPBK10's breast cancer selectivity and intracellular transport properties.

4.2 Corrole-Based Optical Imaging

In addition to their potential utility as anticancer therapeutics, transition metal complexes of the amphipolar corrole **1**-H_3 also are effective scavengers of ROS and RNS, and therefore predicted to be effective in combating oxidative stress related-diseases.[65] The iron(III) corrole **1**-Fe and to a lesser extent **1**-Mn catalyze the decomposition of ROS and RNS and therefore can be used to treat diseases such as diabetes, neurodegeneration, optic neuropathy, and atherosclerosis.[72,73,97,104] The development of effective therapeutic approaches must be guided by detailed cellular uptake and biodistribution data. Optical imaging is a powerful tool for these purposes, and many studies have been performed with **1**-a, as an analogue of the non-fluorescent catalytic antioxidants **1**-Fe and **1**-Mn. One key advantage of **1**-a is that its bright emission allows tracking of intracellular transport, even in whole animals without the need for additional fluorescent labels.[98] For example, the uptake of **1**-a has been monitored for both cultured β cells (insulinoma) and primary rat fetal cortical cells using confocal fluorescence.[73] **1**-Ga was found to be distributed primarily in the cytoplasm after cellular uptake.

Confocal microscopy also was used in early studies of cellular uptake of fluorescent corroles in breast cancer cells.[59] MDA-MB-453 cells treated with HerGa at 4 °C displayed intense red fluorescence around the plasma membrane (but not internally), suggesting that HerGa was bound only on cell surfaces at this temperature. At higher temperature (37 °C), fluorescence was observed in the cytosol, thereby demonstrating that HerGa had been internalized. It was proposed that receptor binding occurred at 4 °C and that receptor-mediated endocytosis dominated at 37 °C. While **1**-Ga and its conjugate HerGa have received the most attention, it is important to keep in mind that the free base **1**-H_3 is almost as fluorescent as **1**-Ga, and that **1**-Al is much more so. Even TiO_2-corrole conjugates are fluorescent, a feature that allowed for examination of the cellular uptake of **1**-Al-TiO_2 into luciferase-transfected glioblastoma U87-Luc cells by confocal microscopy.[105]

Fluorescence lifetime imaging microscopy (FLIM) was used to evaluate the uptake of HerGa under different pH conditions as to provide clues that might shed light on the mechanism of endosomal uptake and release. The fluorescence lifetime of HerGa *in vitro* was measured by FLIM over a range of pH values,[106] revealing shorter fluorescence lifetimes under acidic conditions at both room temperature and 37 °C (Figure 5a). This observation provided insight into the mechanism of endosomal release of HerGa *in vivo*. During cellular uptake of HerGa by MDA-MB-435 cells, the fluorescence lifetime declined from 1200 ps to 700 ps over 30 minutes (Figure 5b), after which it slightly increased. The interpretation of these results was that HerGa initially accumulates into acidic plasma membrane associated vesicles, followed by endosomal vesicle escape and subsequent transport to the internal cellular environment.

Distinguishing between fluorophore-specific emission and background cellular autofluorescence is of prime importance (and a non-trivial task) for the proper analysis of optical imaging. This issue was addressed by determining whether HerGa fluorescence lifetime measurements could discriminate between tumor and normal tissue margins.[107] Tumor and normal regions were observed to display differential HerGa-attributed fluorescence, with longer lifetimes found in tumor relative to normal tissue both *in vivo* and *ex vivo* (Figure 6). As hypoxic tumors secrete lactate due to elevated glycolysis, there is a net acidification of the surrounding microenvironment, resulting in shorter HerGa fluorescent lifetimes. These results show that fluorescence lifetime imaging of HerGa has great potential for the delineation of tumor margins.

The biodistribution of **1**-Ga was evaluated in two separate *in vivo* mouse studies, with and without tumor xenografts, and in the former case for both free and conjugated corrole. Intraperitoneal injection of free **1**-Ga into non-tumor-bearing mice revealed accumulation in the pancreas, lung, heart, kidney and liver, as well as in brain vasculature.[109] The whole animal imaging efforts were less conclusive, due to very high autofluoresence. Single tail vein injections of HerGa into female nude mice bearing human epidermal growth factor receptor 2 (HER2)-positive tumors on each flank (followed by observation with a custom-made fluorescence bioimager) were more revealing.[98] While **1**-Ga alone was nonspecifically distributed without any significant tumor targeting, HerGa displayed preferential accumulation in tumors and much lower distribution to extratumoral regions. Real time images acquired after tail vein injection revealed that the HerGa conjugate accumulated at tumor sites within minutes after administration, in contrast to typical observations with porphyrins.[98]

The accumulation of HerGa into various organs, extracted from mice receiving intravenous injection of corroles, was further investigated using multimode optical imaging *ex vivo*.[108] Fluorescence imaging revealed that HerGa predominantly accumulated in tumor and liver (Figure 7a). These studies also addressed the issue of tumor autofluorescence, an inherent limitation for optical imaging studies in cancer. Autofluorescence from tumors excited at 424 nm is typically characterized by broad spectra that overlap with HerGa and **1**-Ga emission spectra, thereby reducing the contrast for detection of HerGa or **1**-Ga by fluorescence intensity imaging. Spectral imaging was therefore applied to achieve better contrast for HerGa detection. Using two-photon excited fluorescence imaging of tumors,

HerGa accumulation could be observed in detail at microscale (Figure 7b). Relative to FLIM, spectral imaging analysis of HerGa offered better quantitative discrimination between tissue autofluorescence and fluorescence attributed to HerGa-targeting. Fluorescence from liver and tumors was clearly shown to originate from HerGa, while emission from other tissues was attributed to autofluorescence. That multimode optical imaging offered complementary and highly resolved information on tumor retention/accumulation of HerGa (intensity and two-photon) (Figure 7a and d), as well as on tissue concentration (spectral) (Figure 7c), confirmed the utility of HerGa-based imaging for the robust delineation and detection of tumors both *in vivo and ex vivo*.

4.3 Whole Animal (Non-invasive) Imaging

Intense metallocorrole fluorescence provides a unique opportunity to monitor tumor targeting *in vivo*. In particular, HerGa was used for whole animal imaging and targeted chemotherapy.[98] A custom fluorescence bioimager (a multimode optical imaging system) was utilized to demonstrate that **1**-Ga fluorescence in treated mice exhibits nonspecific systemic distribution that appeared to be excluded from tumors.[98] The intense **1**-Ga fluorescence clearly indicated general biodistribution of the nonconjugated corrole (Figure 8a, left image). In contrast, HerGa accumulated in the tumor (Figure 8a, right image) with high selectivity (Figure 8b). Interestingly and importantly, accumulation in the tumor sites occurred within a few minutes after administration (Figure 8b).

Because of the promise of HerGa as an imaging agent, its capacity for rapid tumor detection and demarcation *in vivo* was investigated using a ratiometric spectral imaging method (Figure 9, upper).[107] This method uses ratio imaging at different wavelengths corresponding to pure autofluorescence reference signatures and HerGa fluorescence for quantitative measurements. It enhances relatively low contrast (mainly caused by autofluorescence) and aids in identifying preferential HerGa accumulation for tumor detection and delineation. Compared to other *in vivo* methods, quantitative measurement of the preferential tumor accumulation of HerGa by ratiometric spectral imaging allowed enhanced discrimination between HER2-positive breast tumor regions and normal tissue within 30 minutes after intravenous HerGa injection (Figure 9). The relevance to the clinical setting is clear, as it is of utmost importance to determine the location of tumors quickly and accurately. Therefore, it is envisioned that the ratiometric spectral imaging of HerGa can speed up tumor detection and demarcation prior to surgical intervention.

Another imaging modality for tumor detection and delineation *in vivo* is magnetic resonance imaging (MRI), which is the most widely utilized clinical approach. Paramagnetic/superparamagnetic metal chelates are typically used to influence the proton T1 relaxation rates in the tumor environment and enhance image contrast. Although gadolinium chelates are most commonly used for this purpose, concerns about their toxicity have prompted the search for second-generation contrast enhancing agents. To this end, **1**-Mn, **1**-Ga, and **1**-Fe were examined using a 3T magnetic resonance imaging system as to test the suitability of metallocorroles as MRI contrast agents. **1**-Mn exhibited the highest relaxation rates and showed decreased T1 relaxation times as the **1**-Mn concentration increased (Figure 10a, b). **1**-Mn at an accumulation of 1mM in tumors could be clearly identified in the T1-weighted

MR image of a mouse *in vivo* (Figure 10c).[110] Moreover, HerMn obtained via encapsulation of **1**-Mn into the above described tumor-targeting/cell-penetrating protein HerPBK10, accumulated in breast tumors preferentially. HerMn resulted in an increased T1 relaxation rate and decreased relaxation time in tumor regions, thereby enhancing the tumor contrast in the T1-weighted MR image (Figure 10d). It was found that contrast enhancement of tumor regions in the MR mouse image was 20% higher for the HerMn conjugate compared to **1**-Mn (Figure 10e). These results indicate that HerMn can facilitate tumor-selective imaging and further demonstrate that HerMn possesses great potential as an MRI contrast agent for tumor detection and delineation.

4.4 Cytotoxicities of 1-M and its Conjugates

The first report of the cancer cell-killing properties of non-conjugated negatively charged corroles was in 2006, when Agadjanian et al. showed that high (30 μM) concentrations of **1**-Ga reduced 293, HeLa, and MDA-MB-435 cell numbers by 95–100%, whereas low concentrations (0.3–3 μM) exhibited little or no cytotoxicity after several days in cell media.[59] Similar concentrations of **1**-H_3 were not toxic to MDA-MB-435 cells, whereas **1**-Mn had no effect on 293 and HeLa cells. Investigations by the Termini group followed: **1**-Al was found to be more cytotoxic than **1**-Ga against breast (MDA-MB-231) and ovarian (OVCAR-3) carcinoma lines (30 μM dose).[71] Enhanced cytotoxocity was attributed to the more efficient kinetic uptake of **1**-Al relative to **1**-Ga, measured using the ImageXpress Ultra confocal high content analysis system

Water-soluble gold(III) corrole **1**-Au, the latest member of the **1**-M complexes, was introduced in 2014.[64] Its potential as an anticancer drug was evaluated in four cancer cell lines and compared to **1**-Ga and cisplatin. **1**-Au was found to be 5–10 and ~ 2 times more cytotoxic than **1**-Ga and cisplatin, respectively (Tables 1 and 2).[64] **1**-Au also was cytostatic, while **1**-Ga was not. A possible explanation for the differential cytotoxicities of **1**-Au and **1**-Ga was proposed after examining binding to HSA, the most abundant serum protein that often acts as a drug-sequestering agent. Using electrospray ionization-time of flight mass (ESI-TOF) spectrometry and UV-vis spectroscopy, it was shown that **1**-Au binding to HSA was diminished relative to **1**-Ga. The greater availability of **1**-Au in free (unbound) form might hence be responsible for its enhanced cytotoxicity, reminiscent of other cases where serum albumin binding of drugs decreases their efficacy. One such example is [($^{sec\text{-}butyl}$phen)$AuCl_3$], which displays less toxicity *in vitro* (higher IC_{50}) than cisplatin, as well as stronger binding to bovine serum albumin.[111] A revealing comparison can be made between **1**-Au and gold(III) porphyrins. Although **1**-Au is not as cytotoxic as the lipophilic [Au(TPP)]Cl,[112] it is still substantially more cytotoxic than water-soluble gold(III) porphyrins.[113]

The possibility that more lipophilic corroles might exhibit increased cytotoxicity was explored recently.[114] Two negatively-charged derivatives of **1**-Ga -Ga(ACtpfc) and Ga(3-ctpfc)-were prepared (Figure 11). Not only are Ga(ACtpfc) (cLogP = 13.5) and Ga(3-ctpfc) (cLogP = 13.1) more lipophilic than **1**-Ga, they have smaller polar surface areas and lower molecular weights. Consistent with the hypothesis, Ga(ACtpfc) and Ga(3-ctpfc) exhibited

enhanced intracellular uptake (Figure 11) and correspondingly increased cytotoxicity (Table 3) towards the four National Cancer Institute 60 cell lines tested.

Another recent study explored the cytotoxicity of corroles covalently bound to TiO_2 nanoparticles.[105] TiO_2 is an especially useful material because it is known to exhibit cytotoxicity under UV irradiation.[113–115] That study focused on dark toxicity, revealing decreased viability of human glioblastoma U87-Luc cells treated with >20 μg/mL of **1**-Al–TiO_2.

The hypothesis that the HerPBK10 carrier protein can enhance therapeutic targeting of **1**-a to breast cancer cells was first validated by *in vitro* experiments using MDA-MB-435 cells. Treatment with 0.5 μM HerGa proved cytotoxic to nearly 60% of the cells after 3 days, whereas **1**-a required a ten-fold higher concentration and seven days to achieve the same level of cytotoxicity.[59] Moreover, HerGa selectively killed HER2-positive MDA-MB-231 human breast cancer cells in the presence of HER2-negative cells.[59] Such specificity is highly desirable for a targeted therapeutic approach with potential applications in personalized medicine. Control experiments disclosed that the HerPBK10 ligand exhibited negligible effects on tumor growth while **1**-Ga alone displayed only modest cytotoxicity. Only the conjugate of HerPBK10 and **1**-Ga, HerGa, prevented tumor growth completely and more markedly decreased tumor volume, at the very low dose of 0.008 mg/kg (Figure 12). Even when compared to systemically administered doxorubicin, HerGa treatment showed greater therapeutic efficacy at a five times lower dose.[98] This extremely effective tumor inhibition/regression in mice was obtained with no detectable off-target effects in various tissues and no carrier protein immunogenicity.

The cytotoxicity of metallocorroles in combination with other standard chemotherapy drugs also was explored.[118–121] **1**-a was found to enhance cytotoxicity of the DNA-intercalating anthracycline drug doxorubicin against DU-145 prostate carcinoma cells. Dual administration of doxorubicin and **1**-a resulted in an approximately three-fold decrease in IC_{50} relative to treatment with doxorubicin alone.[71] Since metallocorroles can form complexes with a diverse assortment of carriers, the association of metallocorroles with doxorubicin seems plausible, analogous to the known association of porphyrin-modified micelles with this drug.[122]

Although not designed for application as a PDT agent, the light-induced cytotoxicity of negatively charged metallocorroles was nevertheless investigated. On top of the very significant dark cytotoxicity of HerGa, an even more effective tumor cell killing was observed following irradiation at 424 nm. The already impressive dark IC_{50} of ~0.1–1 nM was further reduced upon irradiation to ~0.001–0.01 nM (Figure 13a).[123] Morphological examination of 424-nm irradiated HerGa-treated cells revealed pronounced rounding and membrane blebbing. Since cells receiving phosphate buffered saline treatment alone showed no such morphological changes, this finding indicates that light may be used to eliminate cells that survive initial HerGa treatment.

5. Mechanisms of Cancer Cell Killing by Corroles

The mechanisms of cancer cell killing by negatively charged non-conjugated and conjugated corroles are of two primary types; one dependent on superoxide production and the other mediated by light-induced singlet oxygen production.[106] In contrast, the main mechanism of positively charged corrole cytotoxicity has been attributed to stabilization of G-quadruplex DNA, which in turn inhibits telomerase activity (see section 3). Nuclease-like activity of corroles (positively and negatively charged) also has been proposed.

5.1. Superoxide-Mediated and Light-Induced Singlet-Oxygen-Mediated Cell-Death Pathways

HerGa was found to exhibit cell killing of HER2-positive breast cancer cells via two mechanisms; one mediated by superoxide[59] and a light-dependent pathway involving singlet oxygen production.[106] The HerPBK10-mediated cell entry is the same in both pathways (Figure 14a). HerGa, which specifically binds to HER in MDA-MB-435 human breast cancer cells, undergoes endocytosis after receptor binding. Escape of HerGa from endosomes was followed by monitoring changes in the HerGa fluorescence lifetime during cellular uptake (Figure 14b). In agreement with the superoxide-mediated mechanism (Figure 14c), the mitochondrial membrane potential and cytoskeleton were disrupted (Figure 14e and f). In contrast and consistent with the light-induced mediated cell death pathway, irradiation at 424 nm produced singlet oxygen (Figure 14d) and intensified mitochondrial and cytoskeletal damage (Figure 14e and f), resulting in cytochrome c release and subsequent programmed cell death (Figure 14g).

5.2. Mitotic Arrest

The mechanism of cytotoxicity also was investigated for negatively charged non-conjugated corroles. These studies revealed that many cancer cells treated with metallocorroles undergo mitotic arrest.[124–127] High percentages of melanoma (SK-MEL-28) cells treated with **1**-a, **1**-Mn, and **1**-Al displayed late M phase cell cycle arrest. [71] Similar results also were observed in breast and ovarian cancer cells incubated with these metallocorroles. The degree of mitotic arrest was in the order **1**-Al > **1**-Mn > **1**-a. A strong correlation between cytotoxicity and cytostaticity was demonstrated in later experiments that focused on the even more cytotoxic **1**-Au,[64] consistent with mitotic arrest as an important cell death mechanism.

Several gallium corroles, including **1**-a, were proposed as potential inhibitors of heat shock protein (Hsp) 90, and this hypothetical interaction was modeled by computational methods. [128] Because of its important role in proliferation and survival,[129–131] the inhibition of Hsp90 by **1**-a and related analogues could conceivably mitigate cell cycle arrest. This mechanism is plausible, considering that structurally related gold porphyrins were found to target Hsp60.[132]

5.3 Stabilization of G-quadruplex DNA

Several studies examining the utility of cationic corroles for stabilizing G-quadruplexes appeared in the literature,[69,74,79] following the initial report on the interaction of corroles with DNA.[67] Factors that were proposed to contribute to the stabilization of G-quadruplex

structures by metallocorroles include: 1) the cationic and electron-withdrawing moieties attached to the corrole ring interacting with electron-rich G-quadruplex DNA; 2) enhancement of the corrole/DNA interaction by the M(III) center; and 3) matching of the G-quartet topology by corrole saddling.[68] **4**-Mn was found to possess these properties as it has electron-withdrawing pyridinium moieties, a tripositive manganese center, and a relatively planar structure for G-quadruplex binding. Consistent with that structural analysis, **4**-Mn displayed the highest selectivity toward human telomeric sequence 21G and mutated sequence 21Gmu out of all eight corroles studied, including **4**-Cu.[69] Of the several sequences that were examined, the highest selectivity was for the oncogene c-Myc, characterized by an IC_{50} = 2.37μM with regard to the inhibition of its telomerase activity. The binding constant of **4**-Mn to quadruplex DNA was found to be 64 times greater than that observed for binding to double-stranded DNA (ds-DNA).

Motivated by these results, four other cationic isomers (**14**-H_3, **15**-H_3, **16**-H_3, **17**-H_3) of **4**-H_3 (the free-base analogue of **4**-Mn) (Chart 5) were found to be good G-quadruplex stabilizers.[79] Notably, the complex of **15**-H_3 with the G-quadruplex formed by G_4TTA had the highest ΔT_m and the greatest selectivity (502-fold) for c-Myc over ds-DNA. It was suggested that the restricted free rotation of the pyridyl rings imposed by the *N*-methyl groups (ortho- > meta > para) affords favorable interactions and enhanced selectivity for the quadruplex form,[79] which is optimized for that particular isomer. This is reminiscent of the previously described steric constraints for DNA binding imposed by *ortho*-*N*-methyl-pyridylium-substituted porphyrins relative to *para*-*N*-methyl-pyridylium analogues.[133]

Of interest in this regard is the molecular docking simulation of **4**-Ga and c-Myc, the first molecular docking study of corroles with G-quadruplex DNA (Figure 15).[74] One conclusion was that π–π stacking and hydrogen bonding with 5’ quartet guanine bases (Figure 15a) likely contribute to the stabilization of G-quadruplex by **4**-Ga. Furthermore, **4**-Ga binds to c-Myc G-quadruplex DNA via a groove binding mode (Figure 15b).

5.4 DNA Cleavage

In light of the observed DNA-binding properties of corroles, their ability to cleave DNA was investigated as well. It was found that **4**-Mn cleaved plasmid DNA in the presence of H_2O_2.[134] This finding was further confirmed by Zhang and coworkers,[135] who demonstrated that a high-valent (oxo)iron corrole is involved in the oxidative cleavage of plasmid DNA by **1**-Fe. Although an obvious limitation to these experiments is the use of plasmid DNA instead of genomic DNA, studies[136–137] have shown that there is a correlation between plasmid DNA cleavage and the cancerostatic activity of inorganic compounds. Nonetheless, it remains to be seen whether corroles can induce intra-tumoral DNA cleavage in a manner analogous to other anticancer drugs.[138–140]

Although several different reaction pathways have been presented in this section, there is no exclusive route that leads to cancer cell death. Depending on the experimental conditions (such as the presence or absence of light), it is apparent that a combination of factors (superoxide-mediated, singlet-oxygen-mediated, Hsp-inhibition-induced, as well as others) contribute to the end result of mitotic catastrophe - formally defined by Castedo et al as: “a

type of cell death occurring during mitosis, as a result of DNA damage or deranged spindle formation coupled to the debilitation of different checkpoint mechanisms that would normally arrest progression into mitosis and hence suppress catastrophic events until repair has been achieved". [141] As research in this area is growing rapidly, we are confident that the cell-death pathways of corrole-treated cancer cells will soon be much better understood.

6 Concluding Remarks

Corroles function as both therapeutic and imaging agents, with exceptional stability and more readily tunable photophysical properties than porphyrins. Since the 1999 discovery of the first scalable synthesis of H_3(tpfc), many corroles have been shown to have promising cytotoxic and cytostatic activity. They form covalent conjugates with TiO_2 nanoparticles and non-covalent conjugates with proteins such as HerPBK10 for targeted corrole delivery. In addition, they can be employed for PDT if and when the other requirements for therapeutic applications (such as strong absorption in the application relevant wavelengths of 700–800 nm) are satisfied. Work with other carriers, as well as with non-conjugated corroles, is ongoing. We confidently predict that corroles will soon join other key members of the cancer chemotherapeutic arsenal.

ACKNOWLEDGEMENTS

This work was supported by a Caltech-COH grant (J.T., H.B.G., and Z.G.), the AACR-Thomas J. Bardos Science Education Award (R.D.T.), the Basic Science Research Program through the National Research Foundation of Korea (NRF) funded by the Ministry of Science, ICT & Future Planning (NRF-2014R1A1A2054934, NRF-2014M3A9D7070668), and Samsung Research Funding for Future Technology (J.Y.H.). Research in the Beckman Institute Laser Center at Caltech was supported by NIH R01 DK019038, while research performed at the Technion was supported by the Israel Science Foundation.

Biographies

Ruijie D. Teo (Darius) completed his undergraduate training in chemistry at Caltech. He was involved in corrole research during his time at Caltech, working under Professor Harry Gray, Professor John Termini, and Professor Zeev Gross. His passion for bioinorganic chemistry has taken him to Duke University for graduate work under the guidance of Professor Michael Therien and Professor David Beratan.

Jae Youn Hwang received a Ph.D. degree in Biomedical Engineering at the University of Southern California under the direction of Professor Daniel L. Farkas. His dissertation included the development of a multimode optical imaging system for preclinical applications *in vivo* and *ex vivo*. He then worked two years as a postdoctoral fellow at Cedars-Sinai Medical Center, exploring biomedical applications of the multimodal imaging system. After postdoctoral training, he moved to the NIH Resource Center for Medical Ultrasonic Transducer Technology to develop a novel multimodal imaging technology by combining high frequency ultrasound and optical imaging technologies. He is currently an Assistant Professor in the Department of Information and Communication Engineering at DGIST.

John Termini was born and raised in New York, and received B.A., M.S., M.Phil. and Ph.D. degrees in Chemistry at Columbia University. His graduate research was in natural products synthesis and biochemistry under Prof. Koji Nakanishi. He went on to become an American

Cancer Society postdoctoral fellow at Caltech in the laboratory of Professor Peter B. Dervan. He is currently a Professor in the Department of Molecular Medicine at the Beckman Research Institute of City of Hope. His research interests include the role of DNA damage and repair in cancer and diabetes and therapeutic applications of metal containing drugs.

After completing a doctoral thesis on inorganic reaction mechanisms at Northwestern and working on ligand field theory as a postdoc in Copenhagen, Harry Gray joined the chemistry faculty at Columbia University, where in the early 1960s he investigated the electronic structures of metal complexes. He moved to Caltech in 1966, where he is the Arnold O. Beckman Professor of Chemistry and the Founding Director of the Beckman Institute. A Wolf Prize Laureate, he has made many contributions to inorganic photochemistry and biological inorganic chemistry.

Zeev Gross completed a Ph. D. degree in 1988 at Bar-Ilan University under the direction of Professor S. Hoz in the field of Physical Organic Chemistry. He then worked two years as a Fulbright postdoctoral fellow in Professor J. T. Groves group at Princeton University, exploring several aspects of the chemistry of porphyrins and their metal complexes. In 1990 he accepted a position at the Technion, where he is currently Professor of Chemistry and the incumbent of the Blum academic chair. Since 1999, when his group discovered the first facile synthesis of corroles from pyrrole and aldehydes, the focus of his research has been on disclosing unique features of corroles and utilization of their metal complexes in numerous applications.

ABBREVIATIONS USED

Ad5	adenovirus serotype 5
DNA	deoxyribonucleic acid
ds	double-stranded
FDA	Food and Drug Administration
FILM	fluorescence lifetime imaging microscopy
HER	human epidermal growth factor receptor
HDL	high-density lipoprotein
HSA	human serum albumin
Hsp	heat shock protein
LDL	low-density lipoprotein
MRI	magnetic resonance imaging
PDT	photodynamic therapy
RNS	reactive nitrogen species

ROS	reactive oxygen species
ss	single-stranded
UV	ultraviolet
UV−vis	ultraviolet−visible

References

(1). American Cancer Society, The History of Cancer (accessed: 7 September 2015).

(2). World Health Organization, World Cancer Report 2014 (accessed: 7 September 2015).

(3). Cancer Research UK. Worldwide Cancer Statistics http://www.cancerresearchuk.org/health-professional/cancer-statistics/worldwide-cancer#heading-Zero (accessed Aug 28, 2016).

(4). David AR; Zimmerman MR Cancer: An Old Disease, a New Disease or Something in Between? Nat. Rev. Cancer 2010, 10, 728–733. [PubMed: 20814420]

(5). National Cancer Institute. Types of Treatment http://www.cancer.gov/about-cancer/treatment/types (accessed Aug 28, 2016).

(6). DeVita VT; Chu E A History of Cancer Chemotherapy. Cancer Res 2008, 68, 8643–8653. [PubMed: 18974103]

(7). Bild AH; Yao G; Chang JT; Wang Q; Potti A; Chasse D; Joshi M-B; Harpole D; Lancaster JM; Berchuck A et al. Oncogenic Pathway Signatures in Human Cancers as a Guide to Targeted Therapies. Nature 2006, 439, 353–357. [PubMed: 16273092]

(8). El-Bayoumy K; Sinha R; Pinto JT; Rivlin RS Cancer Chemoprevention by Garlic and Garlic-Containing Sulfur and Selenium Compounds. J. Nutr 2006, 136, 864S–869S. [PubMed: 16484582]

(9). Chabner BA Barnett Rosenberg: In Memoriam (1924–2009). Cancer Res 2010, 70, 428–429.

(10). Alderden RA; Hall MD; Hambley TW The Discovery and Development of Cisplatin. J. Chem. Educ 2006, 83, 728.

(11). Ardizzoni A; Boni L; Tiseo M; Fossella FV; Schiller JH; Paesmans M; Radosavljevic D; Paccagnella A; Zatloukal P; Mazzanti P et al. Cisplatin-Versus Carboplatin-Based Chemotherapy in First-Line Treatment of Advanced Non–Small-Cell Lung Cancer: An Individual Patient Data Meta-analysis. Natl. Cancer Inst 2007, 99, 847–857.

(12). Raymond E; Chaney SG; Taamma A; Cvitkovic E Oxaliplatin: A Review of Preclinical and Clinical Studies. Ann. Oncol 1998, 9, 1053–1071. [PubMed: 9834817]

(13). May M Statistics: Attacking an Epidemic. Nature 2014, 509, S50–S51. [PubMed: 24870819]

(14). Cancer Nanotechnology: Small, but Heading for the Big Time. Nat. Rev. Drug Discov 2007, 6, 174–175. [PubMed: 17396287]

(15). Bertrand B; Stefan L; Pirrotta M; Monchaud D; Bodio E; Richard P; Le Gendre P; Warmerdam E; de Jager MH; Groothuis GMM et al. Caffeine-Based Gold(I) N-Heterocyclic Carbenes as Possible Anticancer Agents: Synthesis and Biological Properties. Inorg. Chem 2014, 53, 2296–2303. [PubMed: 24499428]

(16). Sava G; Zorzet S; Turrin C; Vita F; Soranzo M; Zabucchi G; Cocchietto M; Bergamo A; DiGiovine S; Pezzoni G et al. Dual Action of NAMI-A in Inhibition of Solid Tumor Metastasis: Selective Targeting of Metastatic Cells and Binding to Collagen. Clin. Cancer Res 2003, 9, 1898–1905. [PubMed: 12738748]

(17). Liu Z; Romero-Canelón I; Qamar B; Hearn JM; Habtemariam A; Barry NPE; Pizarro AM; Clarkson GJ; Sadler PJ The Potent Oxidant Anticancer Activity of Organoiridium Catalysts. Angew. Chem. Int. Ed 2014, 53, 3941–3946.

(18). Ray S; Mohan R; Singh JK; Samantaray MK; Shaikh MM; Panda D; Ghosh P Anticancer and Antimicrobial Metallopharmaceutical Agents Based on Palladium, Gold, and Silver N-Heterocyclic Carbene Complexes. J. Am. Chem. Soc 2007, 129, 15042–15053. [PubMed: 17988129]

(19). Romero-Canelón I; Sadler PJ Next-Generation Metal Anticancer Complexes: Multitargeting via Redox Modulation. Inorg. Chem 2013, 52, 12276–12291. [PubMed: 23879584]

(20). Medici S; Peana M; Nurchi VM; Lachowicz JI; Crisponi G; Zoroddu MA Noble Metals in Medicine: Latest Advances. Coord. Chem. Rev 2015, 284, 329–350.

(21). Miller MA; Askevold B; Yang KS; Kohler RH; Weissleder R Platinum Compounds for High-Resolution In Vivo Cancer Imaging. ChemMedChem 2014, 9, 1131–1135. [PubMed: 24504646]

(22). Dolmans DEJGJ; Fukumura D; Jain RK Photodynamic Therapy for Cancer. Nat. Rev. Cancer 2003, 3, 380–387. [PubMed: 12724736]

(23). Ethirajan M; Chen Y; Joshi P; Pandey RK The Role of Porphyrin Chemistry in Tumor Imaging and Photodynamic Therapy. Chem. Soc. Rev 2011, 40, 340–362. [PubMed: 20694259]

(24). Xu P; Chen J; Chen Z; Zhou S; Hu P; Chen X; Huang M Receptor-Targeting Phthalocyanine Photosensitizer for Improving Antitumor Photocytotoxicity. PLoS ONE 2012, 7, e37051. [PubMed: 22693566]

(25). Dougherty TJ Studies on the Structure of Porphyrins Contained in Photofrin ll. Photochem. Photobiol 1987, 46, 569–573. [PubMed: 2964650]

(26). De Haas ERM; De Vijlder HC; Sterenborg H; Neumann HAM; Robinson DJ Fractionated Aminolevulinic Acid-Photodynamic Therapy Provides Additional Evidence for the use of PDT for Non-Melanoma Skin Cancer. J Eur. Acad. Dermatol. Venereol 2008, 22, 426–430. [PubMed: 18031503]

(27). Li X; Guo H; Tian Q; Zheng G; Hu Y; Fu Y; Tan H Effects of 5-Aminolevulinic Acid-Mediated Photodynamic Therapy on Antibiotic-Resistant Staphylococcal Biofilm: An In Vitro Study. J. Surg. Res 2013, 184, 1013–1021. [PubMed: 23622723]

(28). Kidwai M; Venktaramanan R; Mohan R; Sapra P Cancer Chemotherapy and Heterocyclic Compounds. Curr. Med. Chem 2002, 9, 1209–1228. [PubMed: 12052173]

(29). Boyle RW; Paquette B; Van Lier JE Biological Activities of Phthalocyanines. XIV. Effect of Hydrophobic Phthalimidomethyl Groups on the In Vivo Phototoxicity and Mechanism of Photodynamic Action of Sulphonated Aluminium Phthalocyanines. Br. J. Cancer 1992, 65, 813–817. [PubMed: 1616852]

(30). Margaron P; Madarnas P; Quellet R; Van Lier JE Biological Activities of Phthalocyanines. XVII. Histopathologic Evidence for Different Mechanisms of EMT-6 Tumor Necrosis Induced by Photodynamic Therapy with Disulfonated Aluminum Phthalocyanine or Photofrin. Anticancer Res 1996, 16, 613–620. [PubMed: 8687105]

(31). Gianferrara T; Bergamo A; Bratsos I; Milani B; Spagnul C; Sava G; Alessio E Ruthenium-Porphyrin Conjugates with Cytotoxic and Phototoxic Antitumor Activity. J. Med. Chem 2010, 53, 4678–4690. [PubMed: 20491441]

(32). Lottner C; Bart K-C; Bernhardt G; Brunner H Soluble Tetraarylporphyrin−Platinum Conjugates as Cytotoxic and Phototoxic Antitumor Agents. J. Med. Chem 2002, 45, 2079–2089. [PubMed: 11985475]

(33). Schulz S; Wong RJ; Kalish FS; Zhao H; Jang KY; Vreman HJ; Stevenson DK Effect of Light Exposure on Metalloporphyrin-Treated Newborn Mice. Pediatr. Res 2012, 72, 161–168. [PubMed: 22580722]

(34). Lin N; Li C; Wang Z; Zhang J; Ye X; Gao W; Wang A; Jin H; Wei J A Safety Study of a Novel Photosensitizer, Sinoporphyrin Sodium, for Photodynamic Therapy in Beagle Dogs. Photochem. Photobiol. Sci 2015, 14, 815–832. [PubMed: 25671327]

(35). Saga Y; Hojo S; Hirai Y Comparison of Demetalation Properties Between Zinc Chlorin and Zinc Porphyrin Derivatives: Effect of Macrocyclic Structures. Bioorg. Med. Chem 2010, 18, 5697–5700. [PubMed: 20620069]

(36). Espenson JH; Christensen RJ Kinetics and Mechanism of the Demetalation of Iron(III) Porphyrins Catalyzed by Iron(II). Inorg. Chem 1977, 16, 2561–2564.

(37). Preihs C; Arambula JF; Magda D; Jeong H; Yoo D; Cheon J; Siddik ZH; Sessler JL Recent Developments in Texaphyrin Chemistry and Drug Discovery. Inorg. Chem 2013, 52, 12184–12192. [PubMed: 23557113]

(38). Sessler JL; Hemmi G; Mody TD; Murai T; Burrell A; Young SW Texaphyrins: Synthesis and Applications. Acc. Chem. Res 1994, 27, 43–50.

(39). Sessler JL; Seidel D Synthetic Expanded Porphyrin Chemistry. Angew. Chem. Int. Ed 2003, 42, 5134–5175.

(40). Sessler JL; Miller RA Texaphyrins: New Drugs with Diverse Clinical Applications in Radiation and Photodynamic Therapy. Biochem. Pharmcol 2000, 59, 733–739.

(41). Johnson AW; Kay IT Pentadehydrocorrin (Corrole) Ring System. Proc. Chem. Soc 1964, 89.

(42). Eschenmoser A Centenary Lecture. (Delivered November 1969). Roads to Corrins. Quart. Rev. Chem. Soc 1970, 24, 366–415.

(43). Gross Z; Galili N; Saltsman I The First Direct Synthesis of Corroles from Pyrrole. Angew. Chem. Int. Ed 1999, 38, 1427–1429.

(44). Hocking RK; George SD; Gross Z; Walker FA; Hodgson KO; Hedman B; Solomon EI Fe L-and K-edge XAS of Low-Spin Ferric Corrole: Bonding and Reactivity Relative to Low-Spin Ferric Porphyrin. Inorg. Chem 2009, 48, 1678–1688. [PubMed: 19149467]

(45). Meier-Callahan AE; Di Bilio AJ; Simkhovich L; Mahammed A; Goldberg I; Gray HB; Gross Z Chromium Corroles in Four Oxidation States. Inorg. Chem 2001, 40, 6788–6793. [PubMed: 11735492]

(46). Gross Z; Gray HB How do Corroles Stabilize High Valent Metals? Comments Inorg. Chem 2006, 27, 61–72.

(47). Yun L; Vazquez-Lima H; Fang H; Yao Z; Geisberger G; Dietl C; Ghosh A; Brothers PJ; Fu X Synthesis and Reactivity Studies of a Tin(II) Corrole Complex. Inorg. Chem 2014, 53, 7047–7054. [PubMed: 24941110]

(48). Gouterman M in The Porphyrins, Vol. III (Ed.: Dolphin D), Academic Press, New York, 1979, pp. 1–165.

(49). Bendix J; Dmochowski IJ; Gray HB; Mahammed A; Simkhovich L; Gross Z Structural, Electrochemical, and Photophysical Properties of Gallium(III) 5,10,15-Tris(pentafluorophenyl)corrole. Angew. Chem. Int. Ed 2000, 39, 4048–4051.

(50). Aviv-Harel I; Gross Z Coordination Chemistry of Corroles with Focus on Main Group Elements. Coord. Chem. Rev 2011, 255, 717–736.

(51). Vestfrid J; Botoshansky M; Palmer JH; Durrell AC; Gray HB; Gross Z Iodinated Aluminum(III) Corroles with Long-Lived Triplet Excited States. J. Am. Chem. Soc 2011, 133, 12899–12901. [PubMed: 21793523]

(52). Ding T; Aleman EA; Modarelli DA; Ziegler CJ Photophysical Properties of a Series of Free-Base Corroles. J. Phys. Chem. A 2005, 109, 7411–7417. [PubMed: 16834109]

(53). Ventura B; Degli Esposti A; Koszarna B; Gryko DT; Flamigni L Photophysical Characterization of Free-Base Corroles, Promising Chromophores for Light Energy Conversion and Singlet Oxygen Generation. New J. Chem 2005, 29, 1559–1566.

(54). Simkhovich L; Iyer P; Goldberg I; Gross Z Structure and Chemistry of N-Substituted Corroles and Their Rhodium (I) and Zinc (II) Metal-Ion Complexes. Chem. Eur. J 2002, 8, 2595–2601. [PubMed: 12180339]

(55). Kadish KM; Ou Z; Adamian VA; Guilard R; Gros CP; Erben C; Will S; Vogel E Corroles with Group 15 Ions. 2. Synthesis and Characterization of Octaethylcorroles Containing a Phosphorus Central Atom. Inorg. Chem 2000, 39, 5675–5682. [PubMed: 11151367]

(56). Liang X; Mack J; Zheng L-M; Shen Z; Kobayashi N Phosphorus(V)-Corrole: Synthesis, Spectroscopic Properties, Theoretical Calculations, and Potential Utility for in Vivo Applications in Living Cells. Inorg. Chem 2014, 53, 2797–2802. [PubMed: 24597460]

(57). Pohl J; Saltsman I; Mahammed A; Gross Z; Röder B Inhibition of Green Algae Growth by Corrole-Based Photosensitizers. J. Appl. Microbiol 2015, 118, 305–312. [PubMed: 25385448]

(58). Blumenfeld CM; Grubbs RH; Moats RA; Gray HB; Sorasaenee K Decorating Metal Oxide Surfaces with Fluorescent Chlorosulfonated Corroles. Inorg. Chem 2013, 52, 4774–4776. [PubMed: 23611256]

(59). Agadjanian H; Weaver J; Mahammed A; Rentsendorj A; Bass S; Kim J; Dmochowski I; Margalit R; Gray HB; Gross Z et al. Specific Delivery of Corroles to Cells via Noncovalent Conjugates with Viral Proteins. Pharm. Res 2006, 23, 367–377. [PubMed: 16411149]

(60). Palmer JH; Durrell AC; Gross Z; Winkler JR; Gray HB Near-IR Phosphorescence of Iridium(III) Corroles at Ambient Temperature. J. Am. Chem. Soc 2010, 132, 9230–9231. [PubMed: 20568752]

(61). Rabinovich E; Goldberg I; Gross Z Gold(I) and Gold(III) Corroles. Chem. Eur. J 2011, 17, 12294–12301. [PubMed: 21972002]

(62). Luobeznova I; Raizman M; Goldberg I; Gross Z Synthesis and Full Characterization of Molybdenum and Antimony Corroles and Utilization of the Latter Complexes as Very Efficient Catalysts for Highly Selective Aerobic Oxygenation Reactions. Inorg. Chem 2006, 45, 386–394. [PubMed: 16390079]

(63). Mahammed A; Gray HB; Weaver JJ; Sorasaenee K; Gross Z Amphiphilic Corroles Bind Tightly to Human Serum Albumin. Bioconjugate Chem 2004, 15, 738–746.

(64). Teo RD; Gray HB; Lim P; Termini J; Domeshek E; Gross Z A Cytotoxic and Cytostatic Gold(III) Corrole. Chem. Commun, 2014, 50, 13789–13792.

(65). Haber A; Aviram M; Gross Z Protecting the Beneficial Functionality of Lipoproteins by 1-Fe, a Corrole-Based Catalytic Antioxidant. Chem. Sci 2011, 2, 295–302.

(66). Aviezer D; Cotton S; David M; Segev A; Khaselev N; Galili N; Gross Z; Yayon A Porphyrin Analogues as Novel Antagonists of Fibroblast Growth Factor and Vascular Endothelial Growth Factor Receptor Binding that Inhibit Endothelial Cell Proliferation, Tumor Progression, and Metastasis. Cancer Res 2000, 60, 2973–2980. [PubMed: 10850445]

(67). Gershman Z; Goldberg I; Gross Z DNA Binding and Catalytic Properties of Positively Charged Corroles. Angew. Chem. Int. Ed 2007, 46, 4320–4324.

(68). Fu B; Huang J; Ren L; Weng X; Zhou Y; Du Y; Wu X; Zhou X; Yang G Cationic Corrole Derivatives: A New Family of G-Quadruplex Inducing and Stabilizing Ligands. Chem. Commun 2007, 3264–3266.

(69). Fu B; Zhang D; Weng X; Zhang M; Ma H; Ma Y; Zhou X Cationic Metal–Corrole Complexes: Design, Synthesis, and Properties of Guanine-Quadruplex Stabilizers. Chem. Eur. J 2008, 14, 9431–9441. [PubMed: 18752229]

(70). D'Urso A; Nardis S; Pomarico G; Fragalà ME; Paolesse R; Purrello R Interaction of Tricationic Corroles with Single/Double Helix of Homopolymeric Nucleic Acids and DNA. J. Am. Chem. Soc 2013, 135, 8632–8638. [PubMed: 23692291]

(71). Lim P; Mahammed A; Okun Z; Saltsman I; Gross Z; Gray HB; Termini J Differential Cytostatic and Cytotoxic Action of Metallocorroles against Human Cancer Cells: Potential Platforms for Anticancer Drug Development. Chem. Res. Toxicol 2011, 25, 400–409.

(72). Kupershmidt L; Okun Z; Amit T; Mandel S; Saltsman I; Mahammed A; Bar-Am O; Gross Z; Youdim MBH Metallocorroles as Cytoprotective Agents Against Oxidative and Nitrative Stress in Cellular Models of Neurodegeneration. J. Neurochem 2010, 113, 363–373. [PubMed: 20096090]

(73). Okun Z; Kupershmidt L; Amit T; Mandel S; Bar-Am O; Youdim MBH; Gross Z Manganese Corroles Prevent Intracellular Nitration and Subsequent Death of Insulin-Producing Cells. ACS Chem. Biol 2009, 4, 910–914. [PubMed: 19715343]

(74). Zhang Z; Wen J-Y; Lv B-B; Li X; Ying X; Wang Y-J; Zhang H-T; Wang H; Liu H-Y; Chang CK Photocytotoxicity and G-quadruplex DNA Interaction of Water-Soluble Gallium(III) Tris(N-methyl-4-pyridyl)corrole Complex. Appl. Organometal. Chem 2015, 30, 132–139.

(75). Kumar A; Goldberg I; Botoshansky M; Buchman Y; Gross Z Oxygen Atom Transfer Reactions from Isolated (Oxo)Manganese(V) Corroles to Sulfides. J. Am. Chem. Soc 2010, 132, 15233–15245. [PubMed: 20932015]

(76). Dixon IM; Lopez F; Tejera AM; Estève J-P; Blasco MA; Pratviel G; Meunier B A G-Quadruplex Ligand with 10000-Fold Selectivity over Duplex DNA. J. Am. Chem. Soc 2007, 129, 1502–1503. [PubMed: 17283987]

(77). Burge S; Parkinson GN; Hazel P; Todd AK; Neidle S Quadruplex DNA: Sequence, Topology and Structure. Nucleic Acids Res 2006, 34, 5402–5415. [PubMed: 17012276]

(78). Shuai L; Wang S; Zhang L; Fu B; Zhou X Cationic Porphyrins and Analogues as New DNA Topoisomerase I and II Inhibitors. Chem. Biodivers 2009, 6, 827–837. [PubMed: 19551725]

(79). Ma H; Zhang M; Zhang D; Huang R; Zhao Y; Yang H; Liu Y; Weng X; Zhou Y; Deng M et al. Pyridyl-Substituted Corrole Isomers: Synthesis and their Regulation to G-quadruplex Structures. Chem. Asian J 2010, 5, 114–122. [PubMed: 19937863]

(80). Berlett BS; Stadtman ER Protein Oxidation in Aging, Disease, and Oxidative Stress. J. Biol. Chem 1997, 272, 20313–20316. [PubMed: 9252331]

(81). Sabharwal SS; Schumacker PT Mitochondrial ROS in cancer: initiators, amplifiers or an Achilles' heel? Nat. Rev. Cancer 2014, 14, 709–721. [PubMed: 25342630]

(82). Zhang Y; Wang H; Li J; Jimenez DA; Levitan ES; Aizenman E; Rosenberg PA Peroxynitrite-Induced Neuronal Apoptosis Is Mediated by Intracellular Zinc Release and 12-Lipoxygenase Activation. J. Neurosci 2004, 24, 10616–10627. [PubMed: 15564577]

(83). Fraszczak J; Trad M; Janikashvili N; Cathelin D; Lakomy D; Granci V; Morizot A; Audia S; Micheau O; Lagrost L et al. Peroxynitrite-Dependent Killing of Cancer Cells and Presentation of Released Tumor Antigens by Activated Dendritic Cells. J. Immunol 2010, 184, 1876–1884. [PubMed: 20089706]

(84). Raj L; Ide T; Gurkar AU; Foley M; Schenone M; Li X; Tolliday NJ; Golub TR; Carr SA; Shamji AF et al. Selective killing of cancer cells by a small molecule targeting the stress response to ROS. Nature 2011, 475, 231–234. [PubMed: 21753854]

(85). Waris G; Ahsan H Reactive Oxygen Species: Role in the Development of Cancer and Various Chronic Conditions. J. Carcinog 2006, 5, 14. [PubMed: 16689993]

(86). Trachootham D; Alexandre J; Huang P Targeting Cancer Cells by ROS-Mediated Mechanisms: a Radical Therapeutic Approach? Nat. Rev. Drug Discov 2009, 8, 579–591. [PubMed: 19478820]

(87). Schumacker PT Reactive Oxygen Species in Cancer Cells: Live by the Sword, Die by the Sword. Cancer Cell 2006, 10, 175–176. [PubMed: 16959608]

(88). Sullivan L; Chandel N Mitochondrial Reactive Oxygen Species and Cancer. Cancer Metab 2014, 2, 17. [PubMed: 25671107]

(89). Marullo R; Werner E; Degtyareva N; Moore B; Altavilla G; Ramalingam SS; Doetsch PW Cisplatin Induces a Mitochondrial-ROS Response That Contributes to Cytotoxicity Depending on Mitochondrial Redox Status and Bioenergetic Functions. PLoS ONE 2013, 8, e81162.. [PubMed: 24260552]

(90). Sun S; Han Y; Liu J; Fang Y; Tian Y; Zhou J; Ma D; Wu P Trichostatin A Targets the Mitochondrial Respiratory Chain, Increasing Mitochondrial Reactive Oxygen Species Production to Trigger Apoptosis in Human Breast Cancer Cells. PLoS ONE 2014, 9, e91610. [PubMed: 24626188]

(91). Weinberg SE; Chandel NS Targeting Mitochondria Metabolism for Cancer Therapy. Nat. Chem. Biol 2015, 11, 9–15. [PubMed: 25517383]

(92). Mahammed A; Goldberg I; Gross Z Highly Selective Chlorosulfonation of Tris(pentafluorophenyl)corrole as a Synthetic Tool for the Preparation of Amphiphilic Corroles and Metal Complexes of Chiral Planarity. Org. Lett 2001, 3, 3443–3446. [PubMed: 11678678]

(93). Haber A; Aviram M; Gross Z Variables That Influence Cellular Uptake and Cytotoxic/Cytoprotective Effects of Macrocyclic Iron Complexes. Inorg. Chem 2011, 51, 28–30. [PubMed: 22148393]

(94). Haber A; Agadjanian H; Medina-Kauwe LK; Gross Z Corroles That Bind with High Affinity to Both Apo and Holo Transferrin. J. Inorg. Biochem 2008, 102, 446–457. [PubMed: 18180041]

(95). Merlot AM; Kalinowski DS; Richardson DR Unraveling the Mysteries of Serum Albumin—More Than Just a Serum Protein. Front. Physiol 2014, 5, 299. [PubMed: 25161624]

(96). Bray N Biologics: Transferrin' Bispecific Antibodies Across the Blood–Brain Barrier. Nat. Rev. Drug Discov 2015, 14, 14–15.

(97). Haber A; Mahammed A; Fuhrman B; Volkova N; Coleman R; Hayek T; Aviram M; Gross Z Amphiphilic/Bipolar Metallocorroles That Catalyze the Decomposition of Reactive Oxygen and Nitrogen Species, Rescue Lipoproteins from Oxidative Damage, and Attenuate Atherosclerosis in Mice. Angew. Chem. Int. Ed 2008, 47, 7896–7900.

(98). Agadjanian H; Ma J; Rentsendorj A; Valluripalli V; Hwang JY; Mahammed A; Farkas DL; Gray HB; Gross Z; Medina-Kauwe L Tumor Detection and Elimination by a Targeted Gallium Corrole. Proc. Natl. Acad. Sci 2009, 106, 6105–6110. [PubMed: 19342490]

(99). Paulson AK; Linklater ES; Berghuis BD; App CA; Oostendorp LD; Paulson JE; Pettinga JE; Melnik MK; Vande Woude GF; Graveel BR MET and ERBB2 Are Coexpressed in ERBB2^{+} Breast Cancer and Contribute to Innate Resistance. Mol. Cancer Res 2013, 11, 1112–1121. [PubMed: 23825050]

(100). McGuirk S; Gravel S-P; Deblois G; Papadopoli D; Faubert B; Wegner A; Hiller K; Avizonis D; Akavia U; Jones R et al. PGC-1α Supports Glutamine Metabolism in Breast Cancer. Cancer Metab 2013, 1, 22. [PubMed: 24304688]

(101). Lowenstein PR With a Little Help From My f(X)riends!: The Basis of Ad5-Mediated Transduction of the Liver Revealed. Mol. Ther 2008, 16, 1004–1006. [PubMed: 18500239]

(102). Kalyuzhniy O; Di Paolo NC; Silvestry M; Hofherr SE; Barry MA; Stewart PL; Shayakhmetov DM Adenovirus Serotype 5 Hexon is Critical for Virus Infection of Hepatocytes In Vivo. Proc. Natl. Acad. Sci 2008, 105, 5483–5488. [PubMed: 18391209]

(103). Medina-Kauwe LK; Xie J; Hamm-Alvarez S Intracellular Trafficking of Nonviral Vectors. Gene Ther 2005, 12, 1734–1751. [PubMed: 16079885]

(104). Kanamori A; Catrinescu MM; Mahammed A; Gross Z; Levin LA Neuroprotection Against Superoxide Anion Radical by Metallocorroles in Cellular and Murine Models of Optic Neuropathy. J. Neurochem 2010, 114, 488–498. [PubMed: 20456018]

(105). Blumenfeld CM; Sadtler BF; Fernandez GE; Dara L; Nguyen C; Alonso-Valenteen F; Medina-Kauwe L; Moats RA; Lewis NS; Grubbs RH et al. Cellular Uptake and Cytotoxicity of a Near-IR Fluorescent Corrole-TiO_2 Nanoconjugate. J. Inorg. Biochem, 2014, 140, 39–44. [PubMed: 25061689]

(106). Hwang JY; Lubow DJ; Chu D; Ma J; Agadjanian H; Sims J; Gray HB; Gross Z; Farkas DL; Medina-Kauwe LK A Mechanistic Study of Tumor-Targeted Corrole Toxicity. Mol. Pharm 2011, 8, 2233–2243. [PubMed: 21981771]

(107). Hwang JY; Gross Z; Gray HB; Medina-Kauwe LK; Farkas DL Ratiometric Spectral Imaging for Fast Tumor Detection and Chemotherapy Monitoring In Vivo. J. Biomed. Opt 2011, 16, 066007. [PubMed: 21721808]

(108). Hwang JY; Wachsmann-Hogiu S; Ramanujan VK; Ljubimova J; Gross Z; Gray HB; Medina-Kauwe LK, Farkas DL A Multimode Optical Imaging System for Preclinical Applications In Vivo: Technology Development, Multiscale Imaging, and Chemotherapy Assessment. Mol. Imaging Biol 2012, 14, 431–432. [PubMed: 21874388]

(109). Okun Z; Kupershmidt L; BH Youdim M; Gross Z Cellular Uptake and Organ Accumulation of Amphipolar Metallocorroles with Cytoprotective and Cytotoxic Properties. Anticancer Agents Med. Chem 2011, 11, 380–384. [PubMed: 21453243]

(110). Sims JD; Hwang JY; Wagner S; Alonso-Valenteen F; Hanson C; Taguiam JM; Polo R; Harutyunyan I; Karapetyan G; Sorasaenee K et al. A Corrole Nanobiologic Elicits Tissue-Activated MRI Contrast Enhancement and Tumor-Targeted Toxicity. J. Control. Release 2015, 217, 92–101. [PubMed: 26334483]

(111). Sanghvi CD; Olsen PM; Elix C; Peng S; Wang D; Chen Z; Shin DM; Hardcastle KI; MacBeth CE; Eichler JF Antitumor Properties of Five-Coordinate Gold(III) Complexes Bearing Substituted Polypyridyl Ligands. J. Inorg. Biochem 2013, 128, 68–76. [PubMed: 23948576]

(112). Che C-M; Sun RW-Y; Yu W-Y; Ko C-B; Zhu N; Sun H Gold(III) Porphyrins as a New Class of Anticancer Drugs: Cytotoxicity, DNA Binding and Induction of Apoptosis in Human Cervix Epitheloid Cancer Cells. Chem. Commun 2003, 1718–1719.

(113). Sun RW-Y; Che C-M The Anti-Cancer Properties of Gold(III) Compounds with Dianionic Porphyrin and Tetradentate Ligands. Coord. Chem. Rev 2009, 253, 1682–1691.

(114). Pribisko M; Palmer J; Grubbs RH; Gray HB; Termini J; Lim P Cellular Uptake and Anticancer Activity of Carboxylated Gallium Corroles. Proc. Natl. Acad. Sci 2016, 113, E2258–E2266. [PubMed: 27044076]

(115). Imani R; Veranic P; Iglic A; Kreft ME; Pazoki M; Hudoklin S Combined Cytotoxic Effect of UV-Irradiation and TiO_2 Microbeads in Normal Urothelial Cells, Low-Grade and High-Grade Urothelial Cancer Cells. Photochem. Photobiol. Sci 2015, 14, 583–590. [PubMed: 25385056]

(116). Cai R; Kubota Y; Shuin T; Sakai H; Hashimoto K; Fujishima A Induction of Cytotoxicity by Photoexcited TiO_2 Particles. Cancer Res 1992, 52, 2346–2348. [PubMed: 1559237]

(117). Petković J; Küzma T; Rade K; Novak S; Filipič M Pre-Irradiation of Anatase TiO_2 Particles with UV Enhances Their Cytotoxic and Genotoxic Potential in Human Hepatoma HepG2 Cells. J. Hazard. Mater 2011, 196, 145–152. [PubMed: 21945684]

(118). Honda M; Miura A; Izumi Y; Kato T; Ryotokuji T; Monma K; Fujiwara J; Egashira H; Nemoto T Doxorubicin, Cisplatin, and Fluorouracil Combination Therapy for Metastatic Esophageal Squamous Cell Carcinoma. Dis. Esophagus 2010, 23, 641–645. [PubMed: 20545978]

(119). Lane D Designer Combination Therapy for Cancer. Nat. Biotech 2006, 24, 163–164.

(120). Komarova NL; Boland CR Cancer: Calculated Treatment. Nature 2013, 499, 291–292. [PubMed: 23868257]

(121). Jain RK Normalizing Tumor Vasculature with Anti-Angiogenic Therapy: A New Paradigm for Combination Therapy. Nat. Med 2001, 7, 987–989. [PubMed: 11533692]

(122). Lovell JF; Jin CS; Huynh E; Jin H; Kim C; Rubinstein JL; Chan WCW; Cao W; Wang LV; Zheng G Porphysome Nanovesicles Generated by Porphyrin Bilayers for use as Multimodal Biophotonic Contrast Agents. Nat. Mater 2011, 10, 324–332. [PubMed: 21423187]

(123). Hwang JY; Lubow DJ; Chu D; Sims J; Alonso-Valenteen F; Gray HB; Gross Z; Farkas DL; Medina-Kauwe LK Photoexcitation of Tumor-Targeted Corroles Induces Singlet Oxygen-Mediated Augmentation of Cytotoxicity. J. Control. Release 2012, 163, 368–373. [PubMed: 23041277]

(124). To YF; Sun RW-Y; Chen Y; Chan VS-F; Yu W-Y; Tam PK-H; Che C-M; Lin C-LS Gold(III) Porphyrin Complex is More Potent Than Cisplatin in Inhibiting Growth of Nasopharyngeal Carcinoma In Vitro and In Vivo. Int. J. Cancer 2009, 124, 1971–1979. [PubMed: 19107930]

(125). Chan KS; Koh CG; Li HY Mitosis-Targeted Anti-Cancer Therapies: Where They Stand. Cell Death Dis 2012, 3, e411. [PubMed: 23076219]

(126). Steegmaier M; Hoffmann M; Baum A; Lénárt P; Petronczki M; Krššák M; Gürtler U; Garin-Chesa P; Lieb S; Quant J et al. BI 2536, a Potent and Selective Inhibitor of Polo-Like Kinase 1, Inhibits Tumor Growth In Vivo. Curr. Biol 2007, 17, 316–322. [PubMed: 17291758]

(127). Al Dhaheri Y; Eid A; AbuQamar S; Attoub S; Khasawneh M; Aiche G; Hisaindee S; Iratni R Mitotic Arrest and Apoptosis in Breast Cancer Cells Induced by Origanum Majorana Extract: Upregulation of TNF-α and Downregulation of Survivin and Mutant p53. PLoS ONE 2013, 8, e56649. [PubMed: 23451065]

(128). Teo RD; Dong SS; Gross Z; Gray HB; Goddard WA Computational predictions of corroles as a class of Hsp90 inhibitors. Mol. BioSyst 2015, 11, 2907–2914. [PubMed: 26252737]

(129). Whitesell L; Lindquist SL HSP90 and the Chaperoning of Cancer. Nat. Rev. Cancer 2005, 5, 761–772. [PubMed: 16175177]

(130). Trepel J; Mollapour M; Giaccone G; Neckers L Targeting the Dynamic HSP90 Complex in Cancer. Nat. Rev. Cancer 2010, 10, 537–549. [PubMed: 20651736]

(131). Ciocca DR; Calderwood SK Heat Shock Proteins in Cancer: Diagnostic, Prognostic, Predictive, and Treatment Implications. Cell Stress Chaperones 2005, 10, 86–103. [PubMed: 16038406]

(132). Hu D; Liu Y; Lai Y-T; Tong K-C; Fung Y-M; Lok C-N; Che C-M Anticancer Gold(III) Porphyrins Target Mitochondrial Chaperone Hsp60. Angew. Chem. Int. Ed 2016, 55, 1387–1391.

(133). Shi D-F; Wheelhouse RT; Sun D; Hurley LH Quadruplex-Interactive Agents as Telomerase Inhibitors: Synthesis of Porphyrins and Structure−Activity Relationship for the Inhibition of Telomerase. J. Med. Chem 2001, 44, 4509–4523. [PubMed: 11741471]

(134). Lu J; Liu HY; Shi L; Wang XL; Ying X; Zhang L; Ji LN; Zang LQ; Chang CK DNA Cleavage Mediated by Water-Soluble Manganese Corrole. Chin. Chem. Lett 2011, 22, 101–104.

(135). Zhang Y; Wen J-Y; Mahmood MHR; Wang X-L; Lv B-B; Ying X; Wang H; Ji L-N; Liu H-Y DNA/HSA Interaction and Nuclease Activity of an Iron(III) Amphiphilic Sulfonated Corrole. Luminescence 2015, 30, 1045–1054. [PubMed: 25736221]

(136). Ghosh K; Kumar P; Mohan V; Singh UP; Kasiri S; Mandal SS Nuclease Activity via Self-Activation and Anticancer Activity of a Mononuclear Copper(II) Complex: Novel Role of the Tertiary Butyl Group in the Ligand Frame. Inorg. Chem 2012, 51, 3343–3345. [PubMed: 22372979]

(137). Bhat SS; Kumbhar AA; Heptullah H; Khan AA; Gobre VV; Gejji SP; Puranik VG Synthesis, Electronic Structure, DNA and Protein Binding, DNA Cleavage, and Anticancer Activity of

Fluorophore-Labeled Copper(II) Complexes. Inorg. Chem 2011, 50, 545–558. [PubMed: 21155539]

(138). Epstein RJ Drug-Induced DNA Damage and Tumor Chemosensitivity. J. Clin. Oncol 1990, 8, 2062–2084. [PubMed: 2230898]

(139). Pratviel G; Bernadou J; Meunier B Carbon—Hydrogen Bonds of DNA Sugar Units as Targets for Chemical Nucleases and Drugs. Angew. Chem. Int. Ed 1995, 34, 746–769.

(140). Norbury CJ; Zhivotovsky B DNA damage-induced apoptosis. Oncogene 2004, 23, 2797–2808. [PubMed: 15077143]

(141). Castedo M; Perfettini J-L; Roumier T; Andreau K; Medema R; Kroemer G Oncogene 2004, 23, 2825–2837. [PubMed: 15077146]

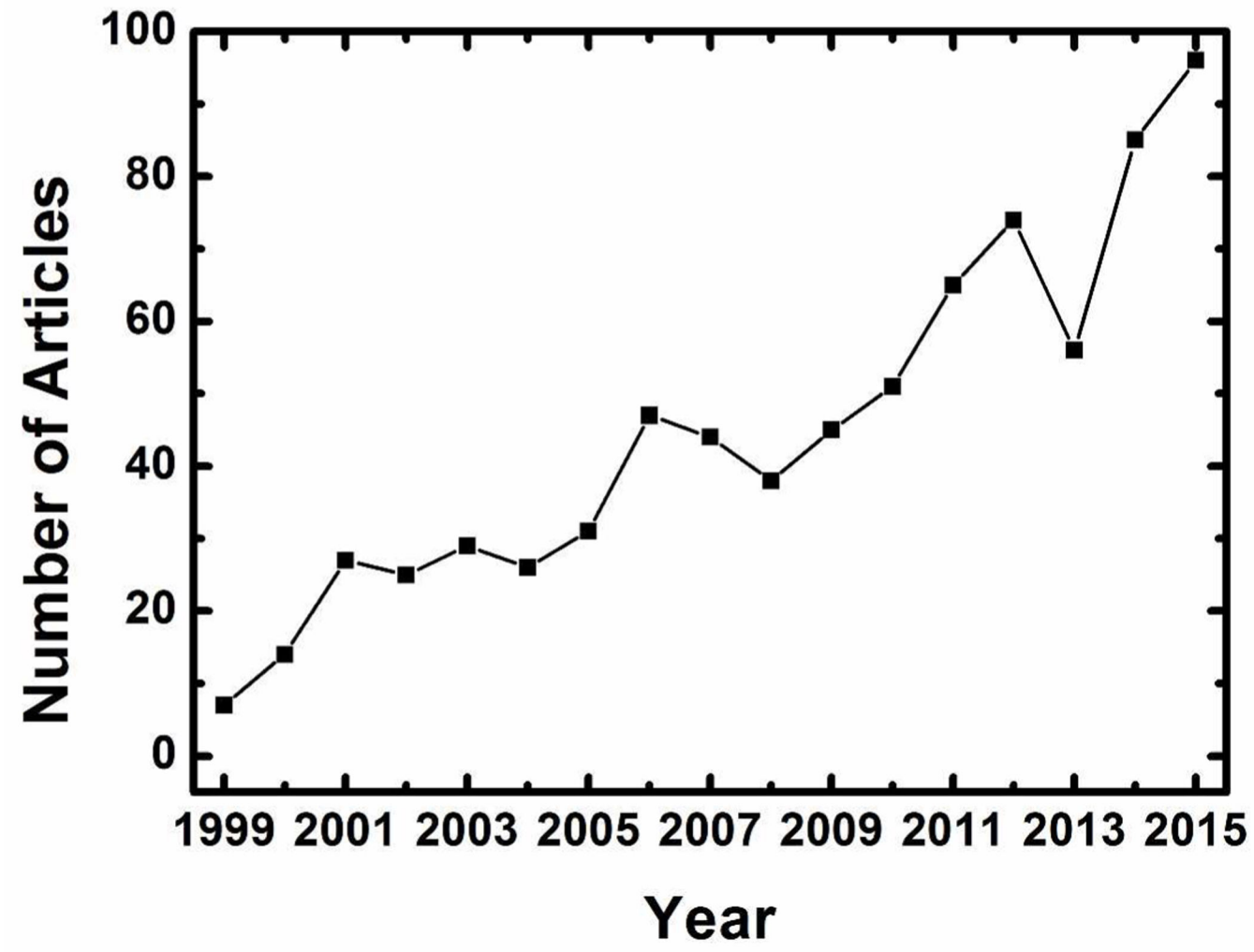

Figure 1.
Published articles per year with keyword “corrole”, based on a Web of Science search conducted on May 4, 2016.

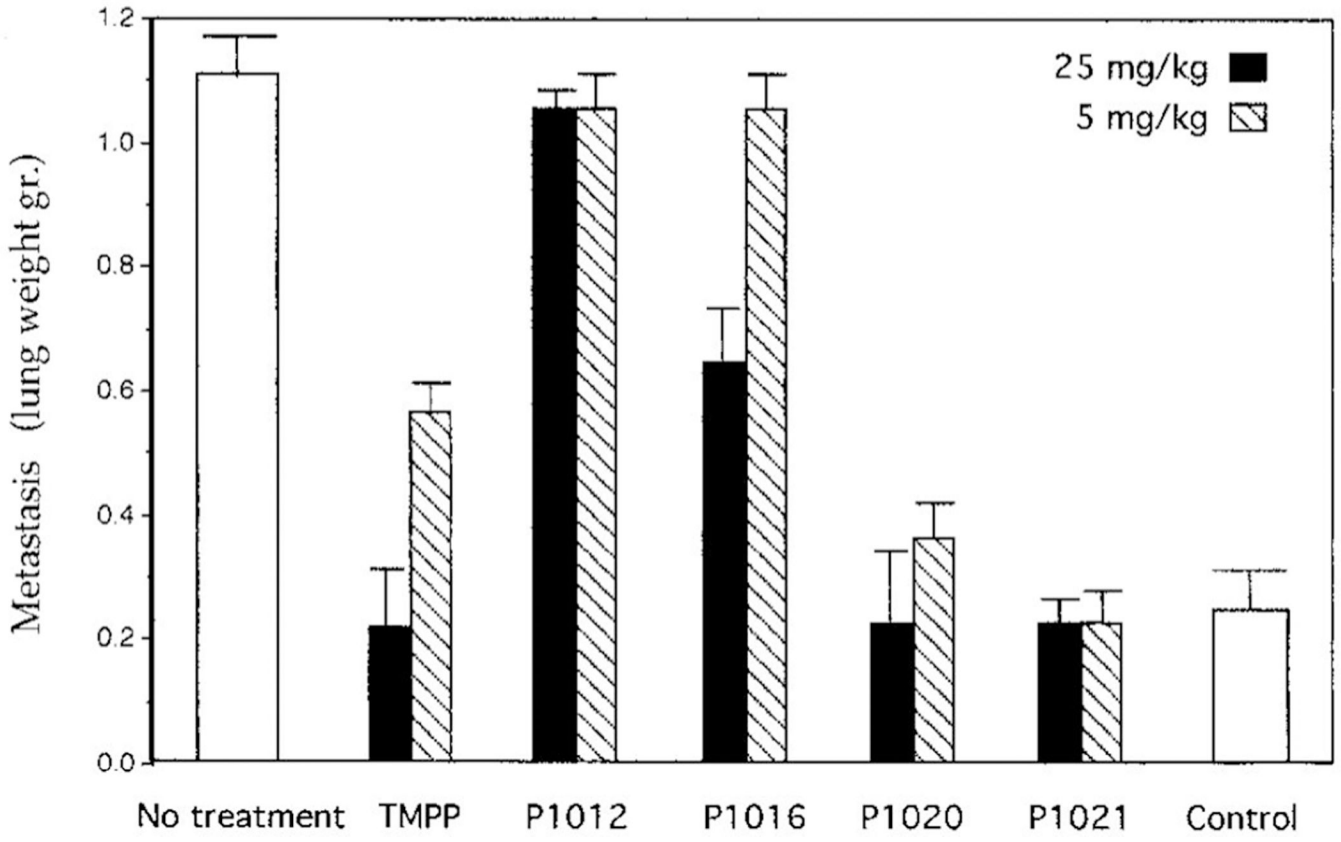

Figure 2.

Inhibition of metastasis in a Lewis lung carcinoma tumor model by the compounds depicted in Scheme 1 (P1021 is the corrole and P1012 is the *ortho*-pyridyl analogue of TMPP). Reproduced from ref. 66. Copyright 2000 American Association for Cancer Research.

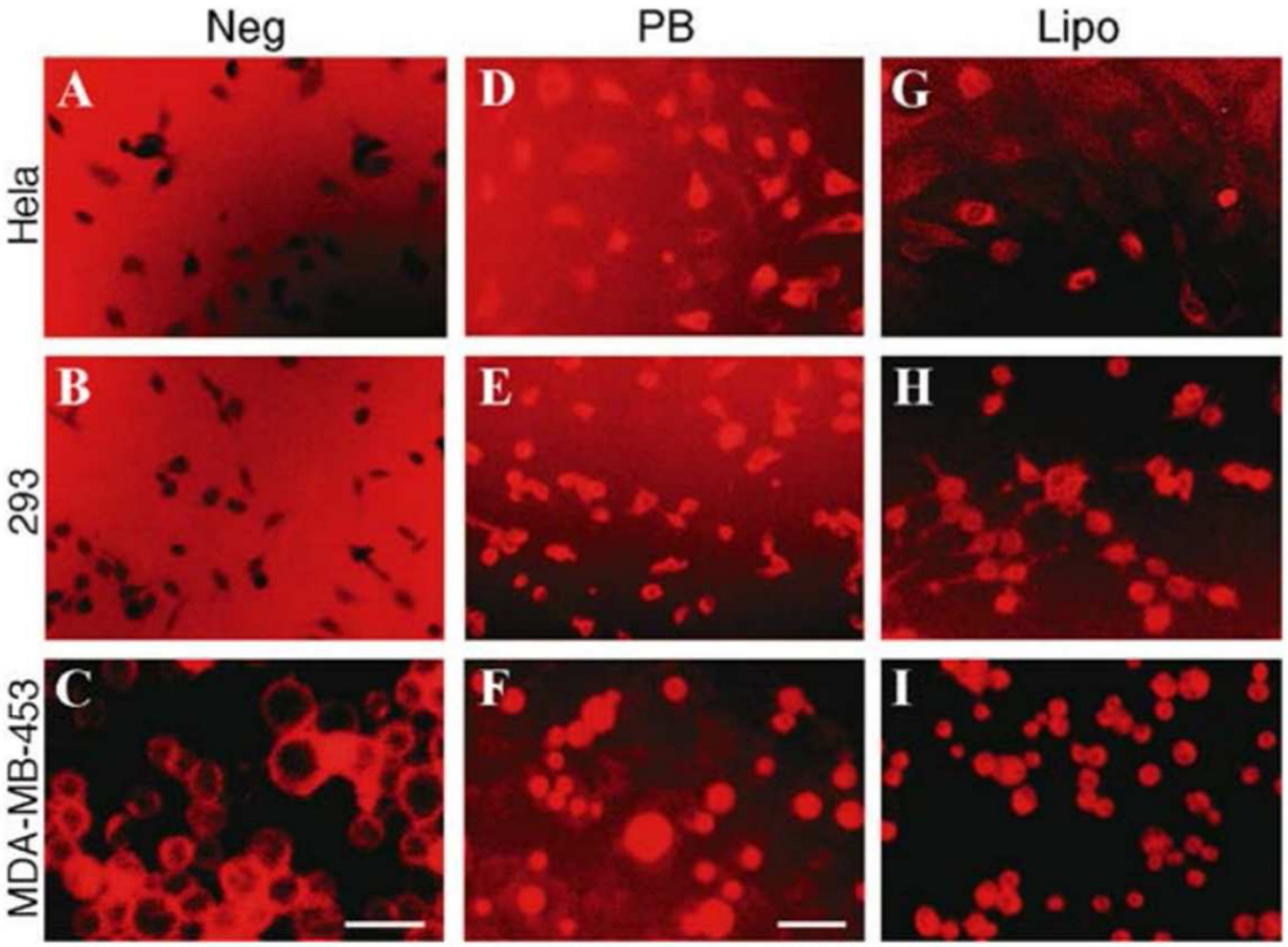

Figure 3.

Uptake of corroles with negatively charged head groups requires a carrier. (a-i) MDA-MB-453, 293 and Hela cells were treated by **1**-a in buffer only (Neg) or with recombinant penton base (PB) or Lipofectin (Lipo). Images were obtained of live cells at 10x magnification using an Olympus IMT-2 inverted microscope fitted with a Texas Red filter. Fluorescence settings were kept constant, and images were captured at constant exposure and gain settings. c and f are slightly enlarged views. Bar, ~20 μm. Reproduced with permission from ref. 59. Copyright 2006 Springer.

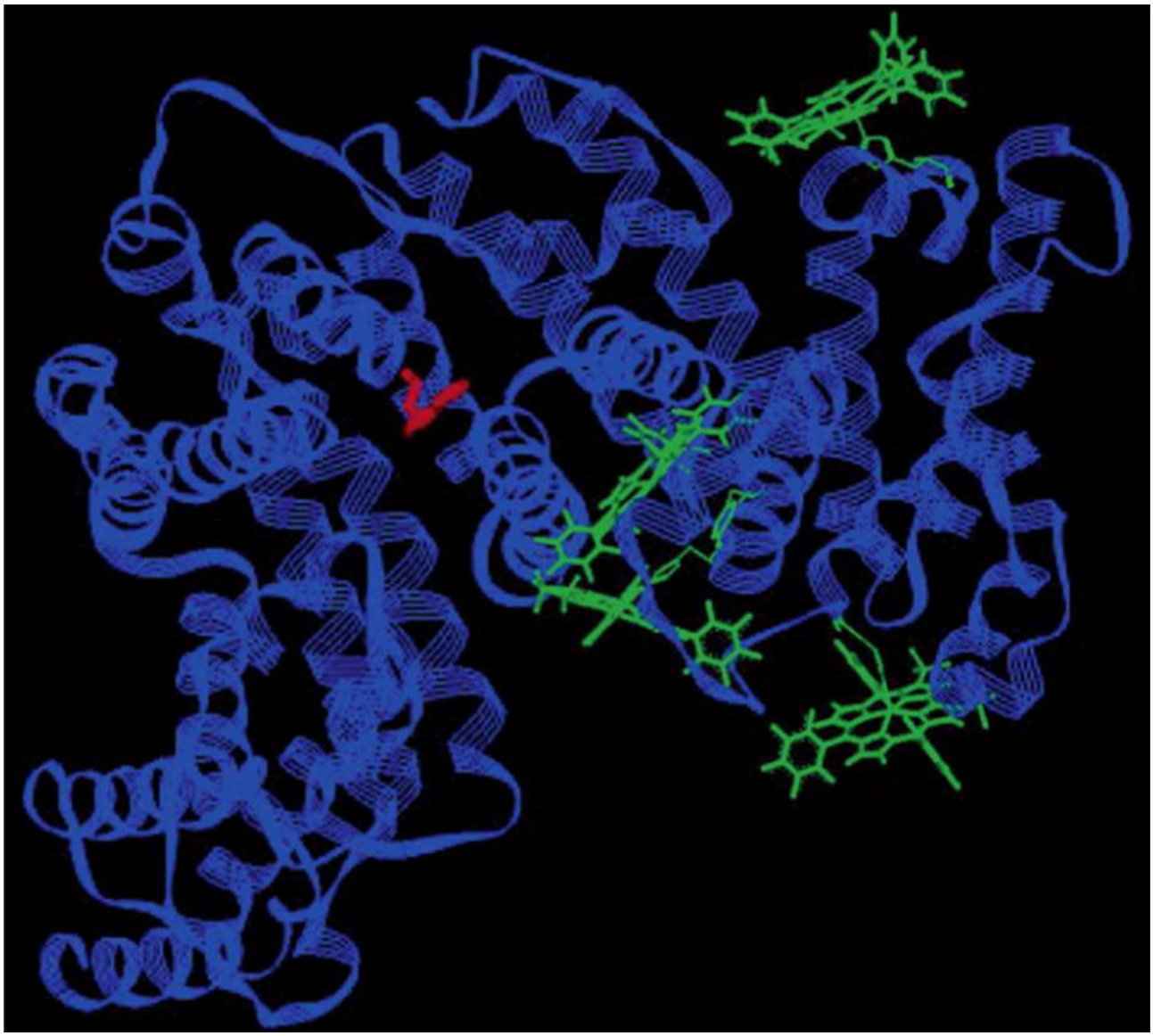

Figure 4.

Structural model depicting four potential binding sites for **1**-Ga (green) in human serum albumin (HSA). The unique tryptophan (Trp^{214}, in red) was used to predict binding sites, based on analysis of fluorescence-quenching data. Reproduced from ref. 63. Copyright 2004 American Chemical Society.

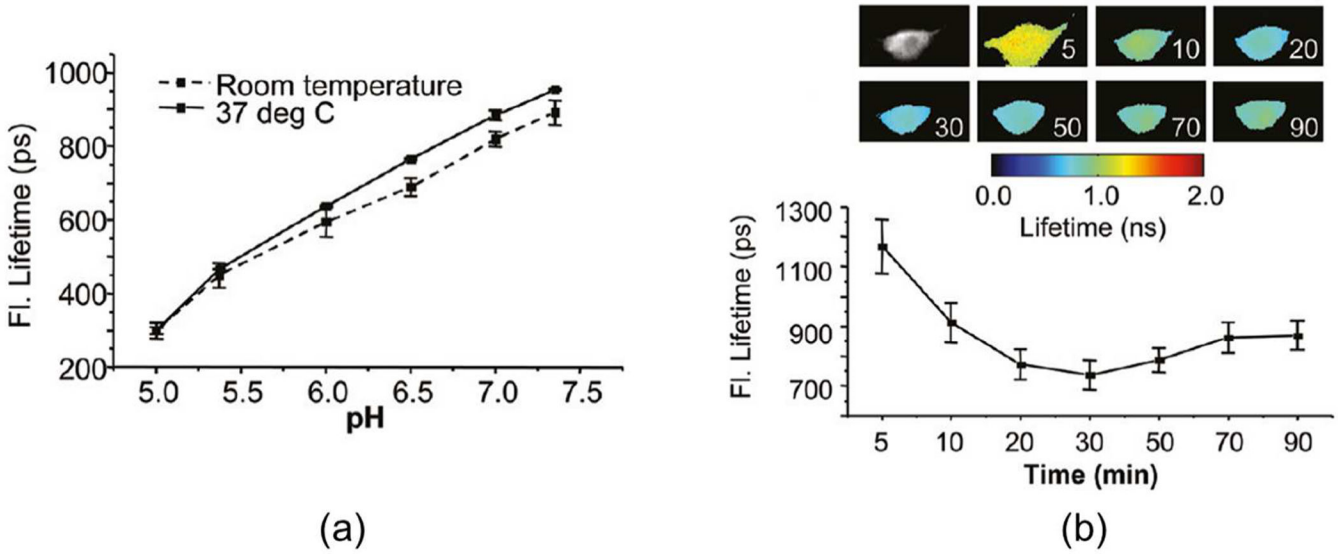

Figure 5. Effect of pH on HerGa fluorescence lifetimes.

(a) Measurement of HerGa fluorescence lifetimes in titrating pH buffers at room temperature and 37 °C (b) Fluorescence lifetime changes of HerGa during uptake into MDA-MB-435 cells. Reproduced from ref. 106. Copyright 2011 American Chemical Society.

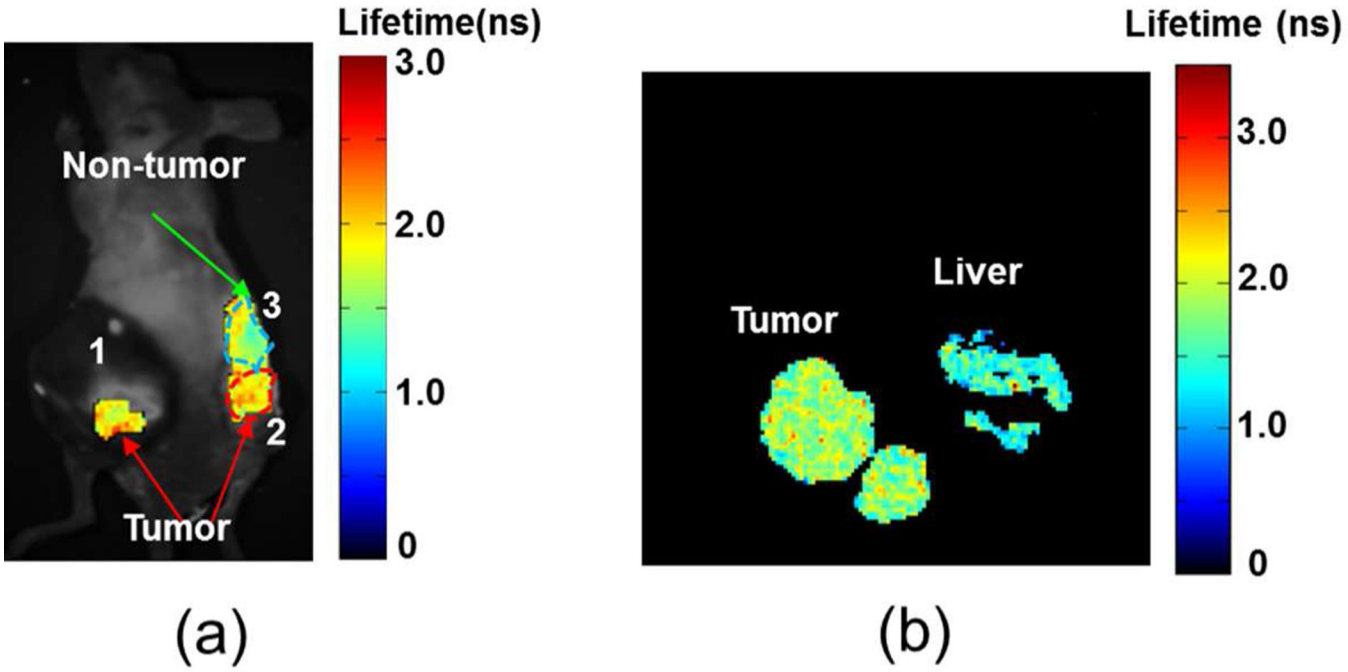

Figure 6.

Tumor detection by fluorescence lifetime imaging of HerGa (a) *in vivo* and *(b) ex vivo*. Reproduced with permission from ref. 108. Copyright 2012 Springer.

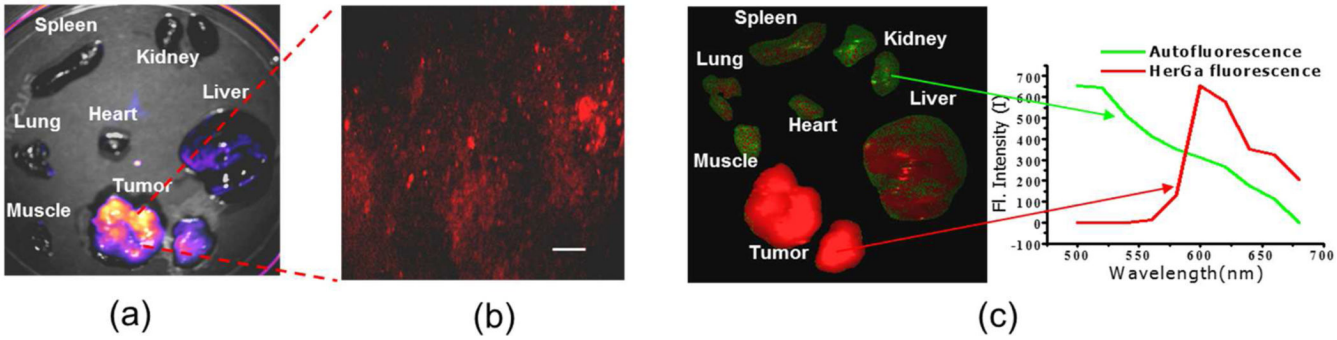

Figure 7.

Tumor detection by multimodal imaging of HerGa. (a) Fluorescence intensity image of organs and tumors at 620 nm. (b) Two-photon excited fluorescence image of tumors. (c) Spectral classified image (left) and spectral signatures (right). Adapted with permission from ref. 108. Copyright 2012 Springer.

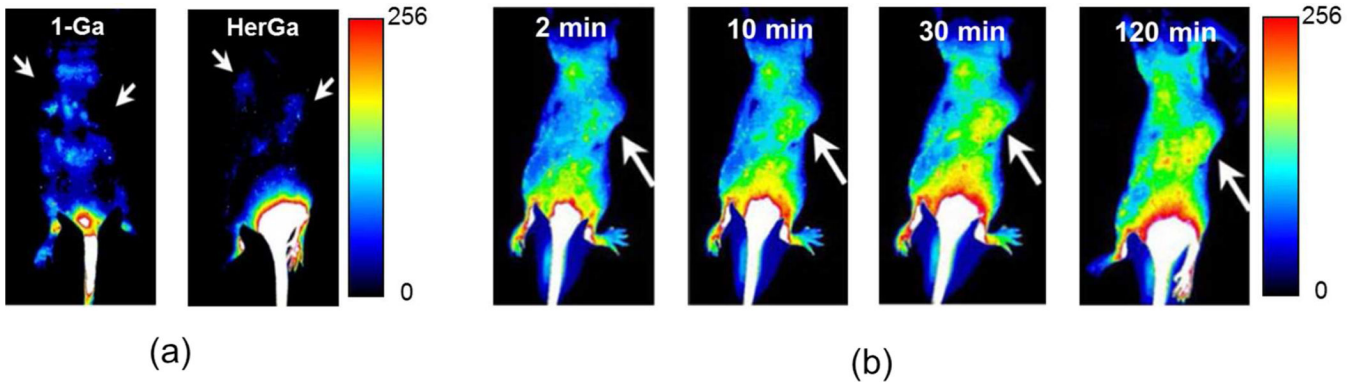

Figure 8.

Targeted tumor detection by fluorescence imaging of HerGa: (a) fluorescence images of nude mice bearing bilateral HER2-positive tumors receiving a single IV injection of either **1**-a or HerGa (b) HerGa distribution over a mouse at the indicated time points after single injection. Adapted from ref. 98. Copyright 2009 National Academy of Sciences.

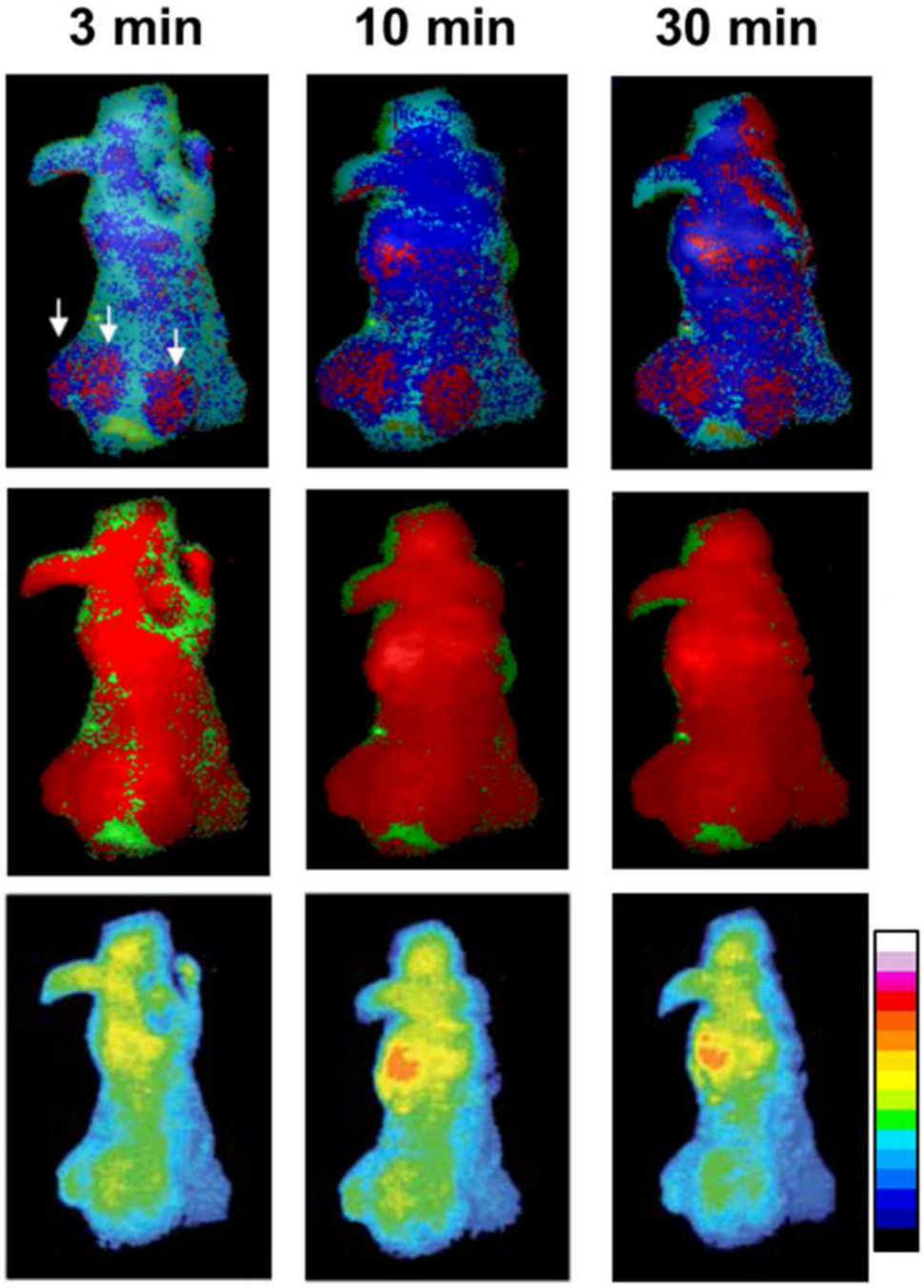

Figure 9.

Tumor detection by ratiometric spectral imaging of HerGa *in vivo*: ratiometric spectral classification (upper), conventional spectral classification (middle), and fluorescence intensity image (lower) of a mouse treated with HerGa at the indicated time points. The arrows indicate tumor regions. Reproduced with permission from ref. 107. Copyright 2011 Society of Photo Optical Instrumentation Engineers.

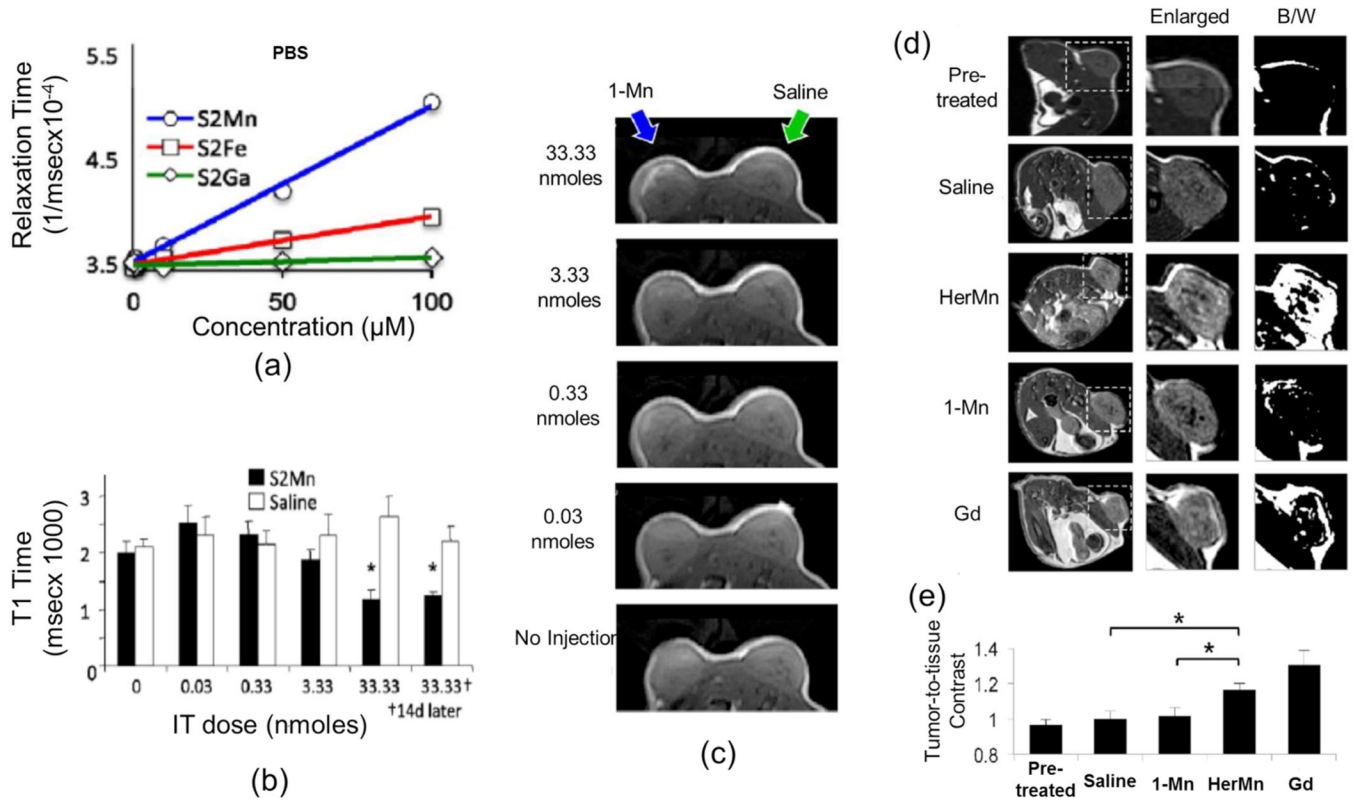

Figure 10.

Tumor detection by MRI of HerMn and the non-conjugated metallocorroles (S2Mn, S2Fe, and S2Ga are identical to **1**-Mn, **1**-Fe, and **1**-Ga, respectively): (a) T1 relaxation ratios of **1**-Mn, **1**-Fe, and **1**-Ga (b) T1 relaxation times of **1**-Mn at different concentrations (c) MR images of a mouse with intratumoral injection of **1**-Mn at different concentrations (d) MR images of tumor-bearing mice before and after IV injection of saline, HerMn, **1**-Mn, and gadolinium(Gd) (e) MRI contrast comparisons between treatment groups (Saline, **1**-Mn, HerMn, and Gd) *in vivo.* Reproduced with permission from ref. 110. Copyright 2015 Elsevier.

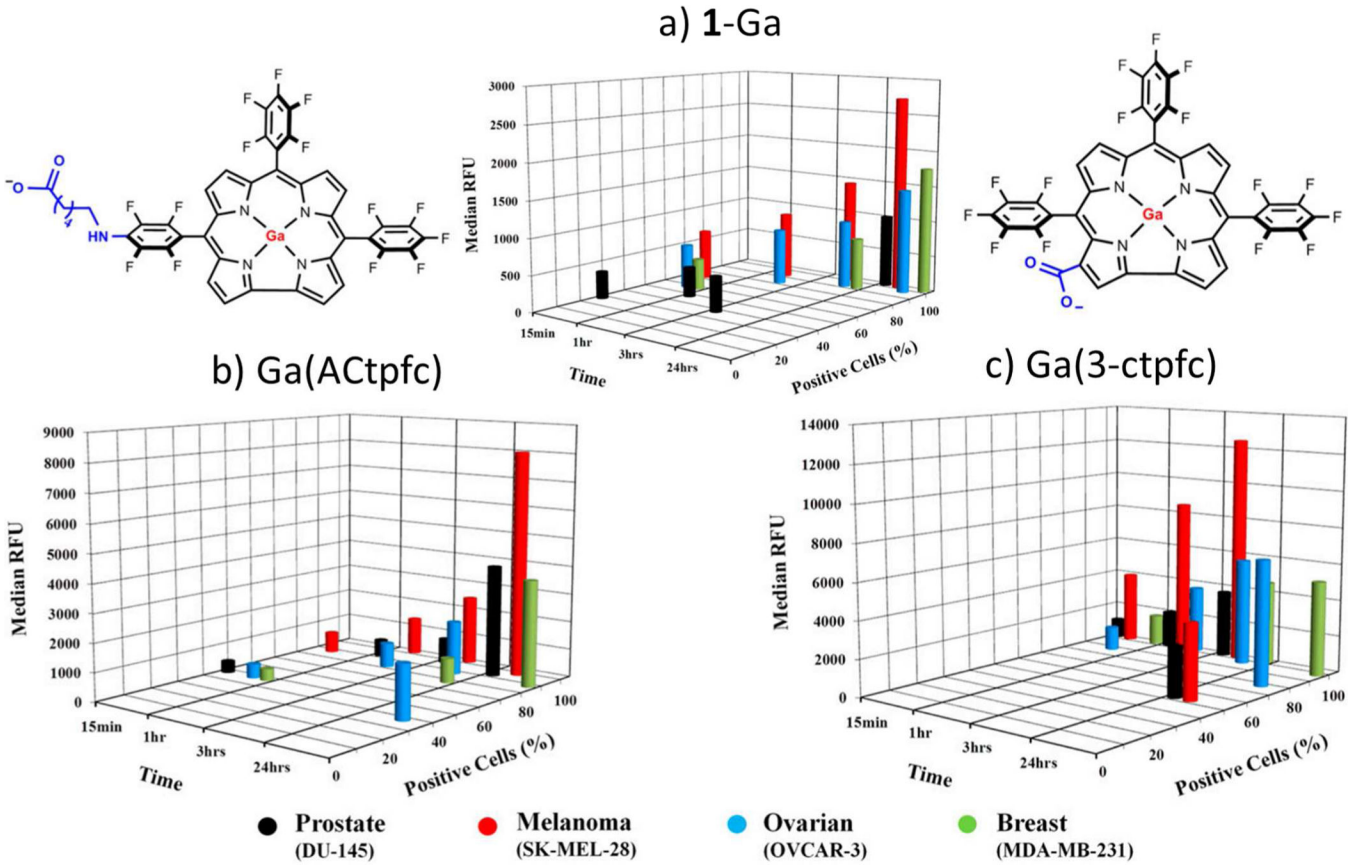

Figure 11.

Kinetics of intracellular uptake and accumulation of **1**-Ga and its derivatives by DU-145 (black), SK-MEL-28 (red), OVCAR-3 (blue), and MDA-MB-231 (green) cancer cells, determined using the ImageExpress Ultra system. Cells were treated with 30 μM (A) **1**-Ga, (B) Ga(ACtpfc), or (C) Ga(3-ctpfc) for the times indicated on the x axis. The y-axis represents a percentage of corrole-positive cells with observable intracellular red fluorescence. The extent of corrole uptake and intracellular accumulation was directly proportional to the median fluorescence intensity (RFU) on the z axis. Cell images were obtained at 20× magnification, using filters for blue (DAPI) and red fluorescence. Adapted from ref. 114. Copyright 2016 National Academy of Sciences.

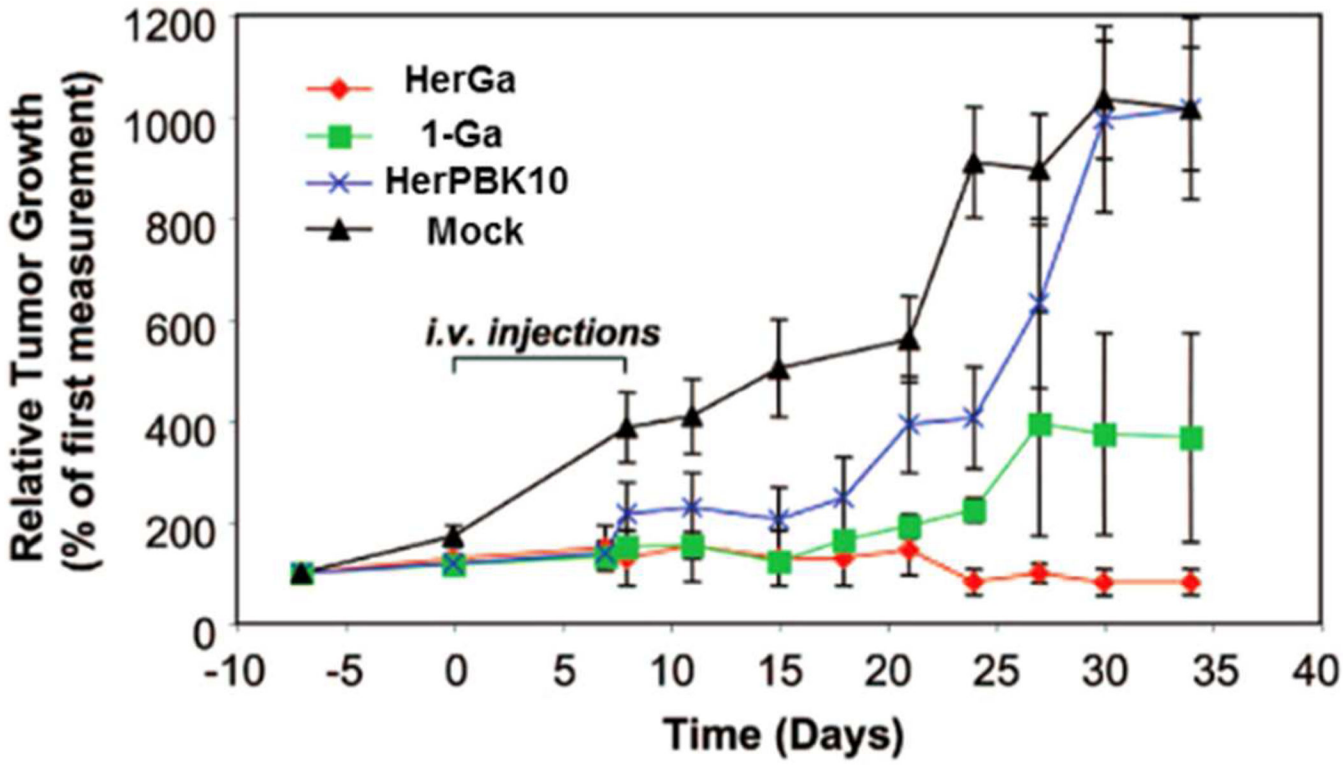

Figure 12.

Targeted tumor elimination: tumor volume changes before, during, and after treatment. Mock treated mice received only saline treatment. Reproduced from ref. 98. Copyright 2009 National Academy of Sciences.

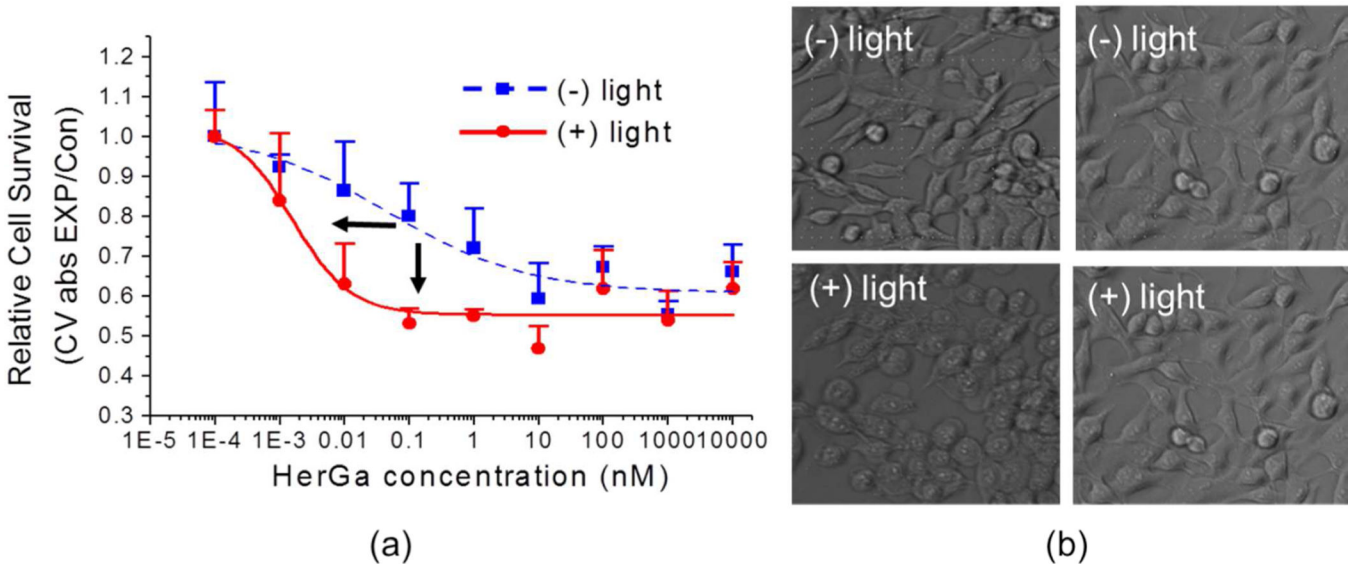

Figure 13.

Cytotoxicity of HerGa in MDA-MB-231 cells with and without irradiation at 424 nm: (a) cell survival at HerGa with and without 424-nm irradiation with the indicated concentrations (b) morphological changes of cancer cells by HerGa treatment with and without light. Reproduced with permission from ref. 123. Copyright 2012 Elsevier.

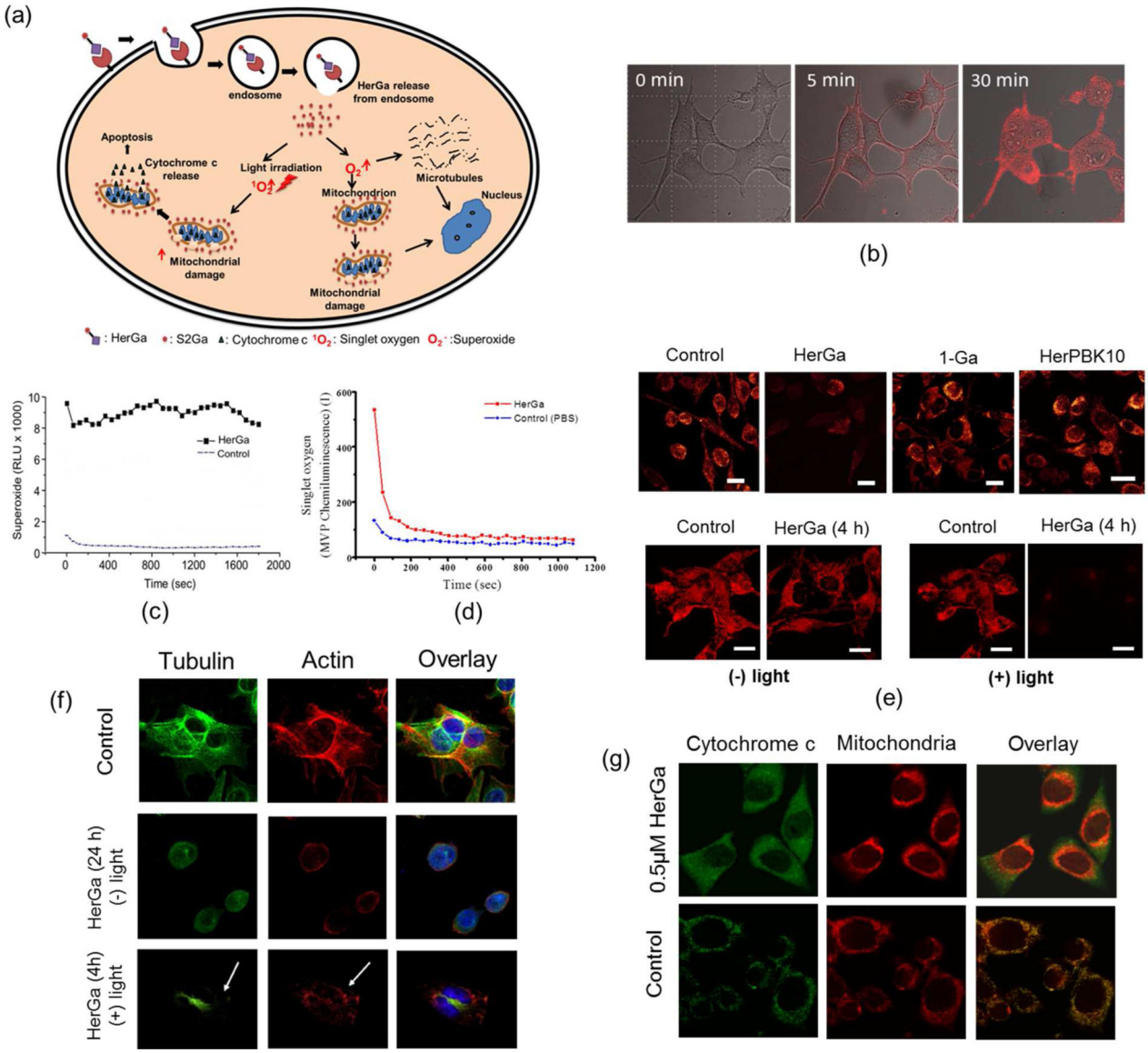

Figure 14.

Cellular mechanisms for cancer cell destruction by HerGa: (a) Schematic of two distinct molecular pathways of HerGa induced cytotoxicity (b) Real time fluorescent images of HerGa internalization in MDA-MB-435 cells. (c) Superoxide generation by cytosolic HerGa (d) singlet oxygen generation following irradiation of HerGa at 424 nm (e) TRMR fluorescence images of MDA-MB-435 cells treated with **1**-a, HerGa, and HerPBK10 for 24 h in the dark (upper) and for 4 h with and without 424-nm irradiation (below) (f) Irradiation of HerGa-induced disruption of major cytoskeletal components tubulin and actin: MDA-MB-435 cells were treated with 1 μM HerGa and irradiated for 4 h at 424 nm. Antibody staining for tubulin (green) and actin (red) revealed major cytoskeletal perturbations after photochemical activation of HerGa, indicated by arrows in the bottom panel. DNA staining with DAPI (blue) showed disruption of the nuclear membrane. Incubation with HerGa in the dark (middle panel) revealed superoxide-mediated microtubule dissociation. (g) cytochrome

c release from 0.5 μM HerGa treated cells after 424-nm irradiation.[106, 123] Reproduced with permission from ref. 106 and 123. Copyright 2011 and 2012 American Chemical Society and Elsevier, respectively.

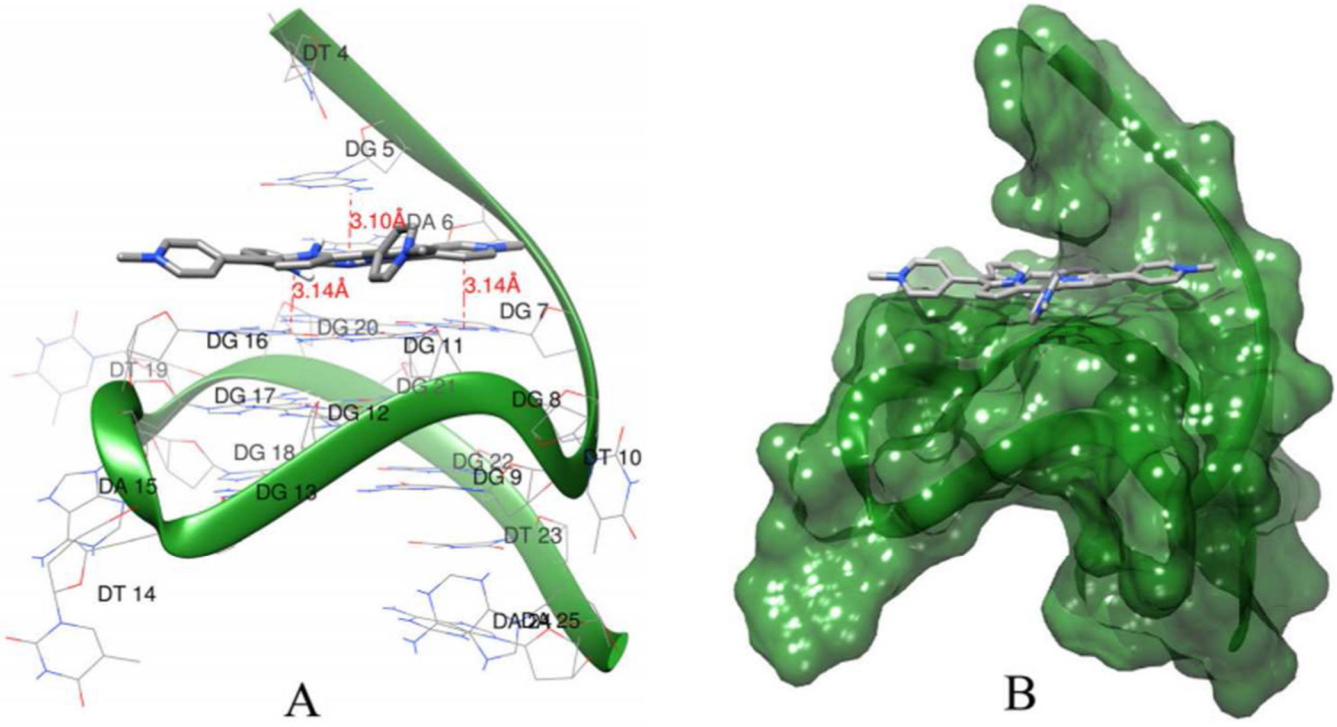

Figure 15.

Results of molecular docking simulations. (a) Hydrogen binding between **4**-Ga and c-Myc G-quadruplex DNA. (b) Binding mode of **4**-Ga with c-Myc G-quadruplex DNA. Reproduced with permission from ref. 74. Copyright 2015 Elsevier.

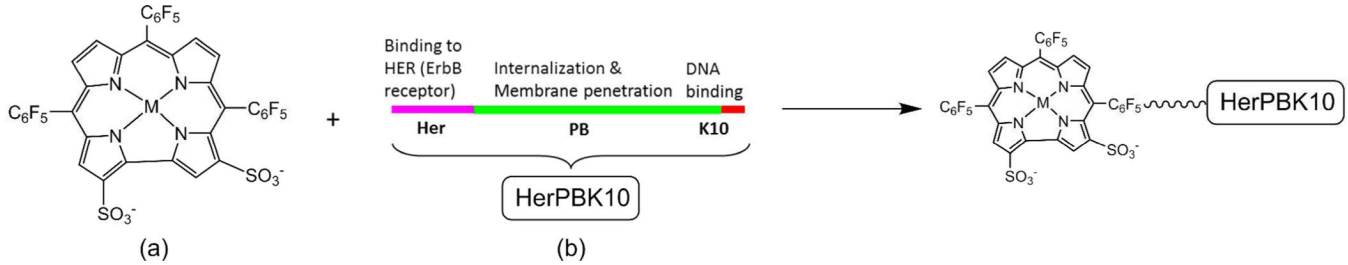

Scheme 1.

Conjugation of metallocorroles for targeting tumors: (a) sulfonated derivatives; (b) tumor targeting cell penetration protein (HerPBK10).

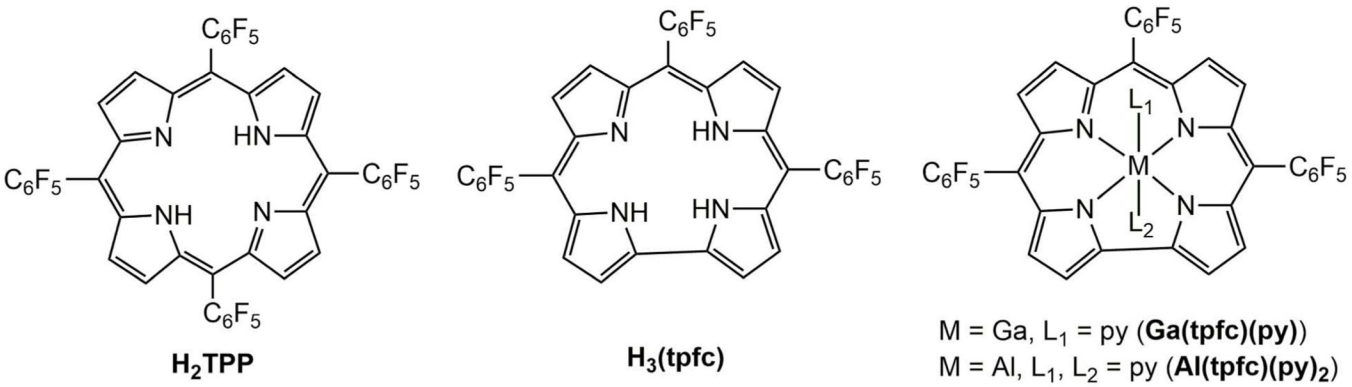

Chart 1.

Structures of 5,10,15,20-tetraphenylporphyrin, 5,10,15-trispentafluorophenyl-corrole, and the corresponding gallium(III) and aluminum(III) corroles. TPP stands for dianionic porphyrin and tpfc for trianionic corrole.

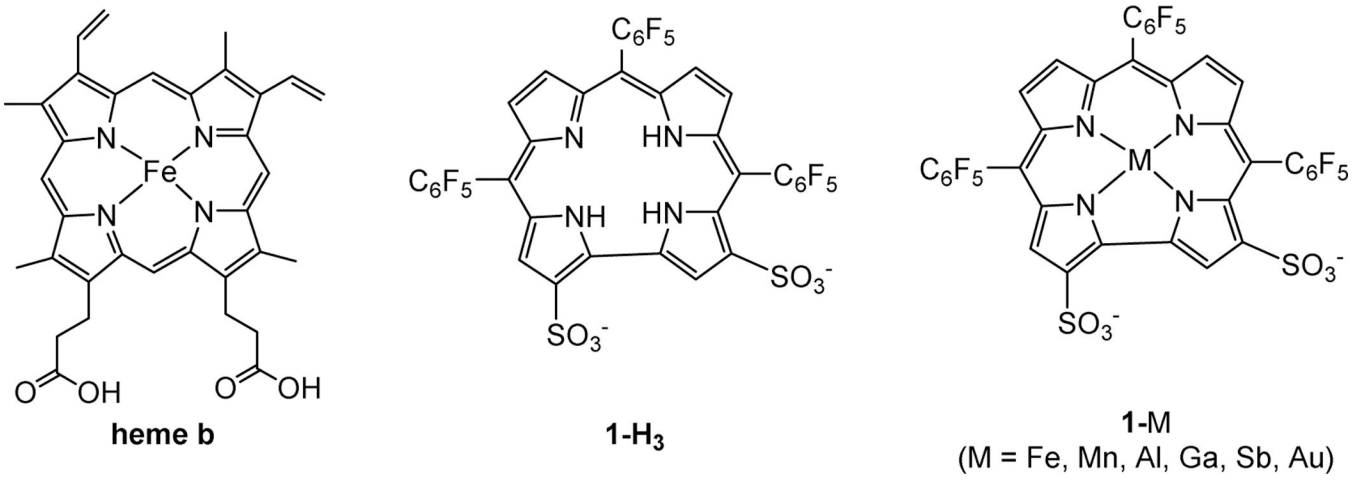

Chart 2.

Structures of heme b (the iron(II) complex of protoporphyrin IX), amphipolar corrole **1**-H_3 and its metal complexes (**1**-M, where M is a tripositive transition metal or post-transition element ion), which are the most thoroughly investigated metallocorroles for therapy.

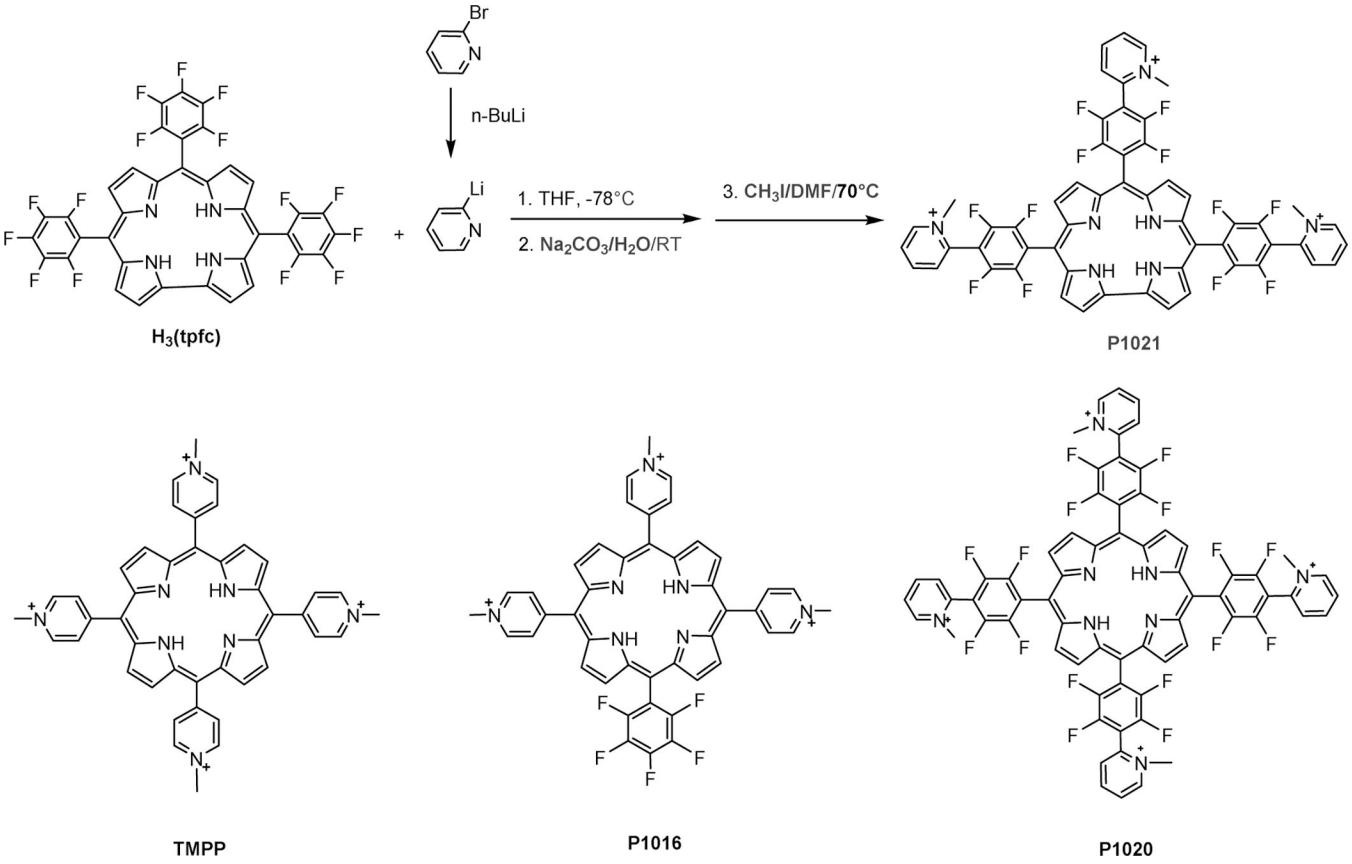

Chart 3.

Synthesis of the first corrole that was included in a cancer-relevant investigation (P1021); the activity of P1021 was compared with those of four porphyrins (the structures of three are shown).[66]

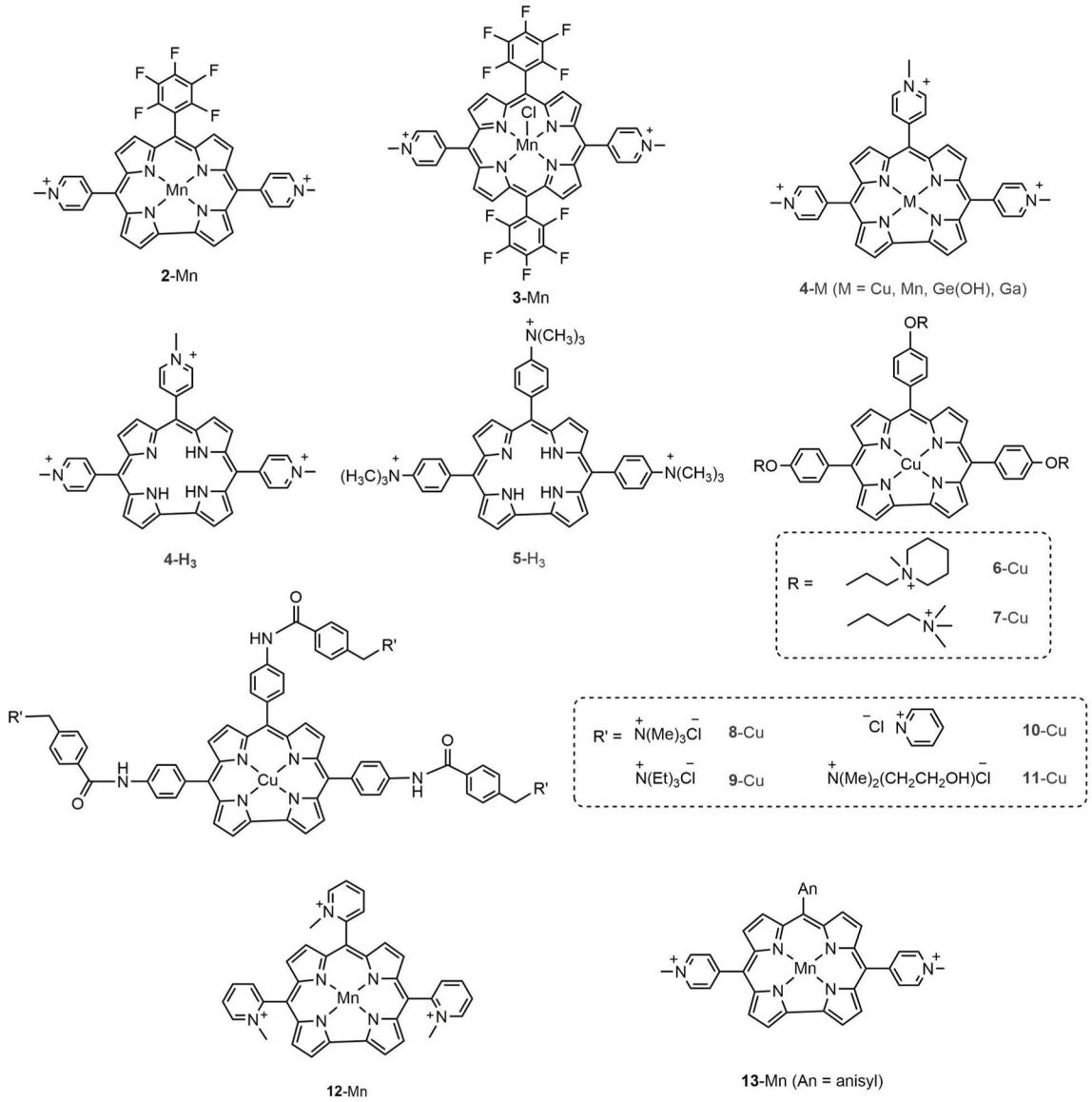

Chart 4.

Structures of corroles with positively charged substituents along with corresponding metal complexes, including corrole **2**-Mn for comparison with the analogous porphyrin, **3**-Mn.
67–74

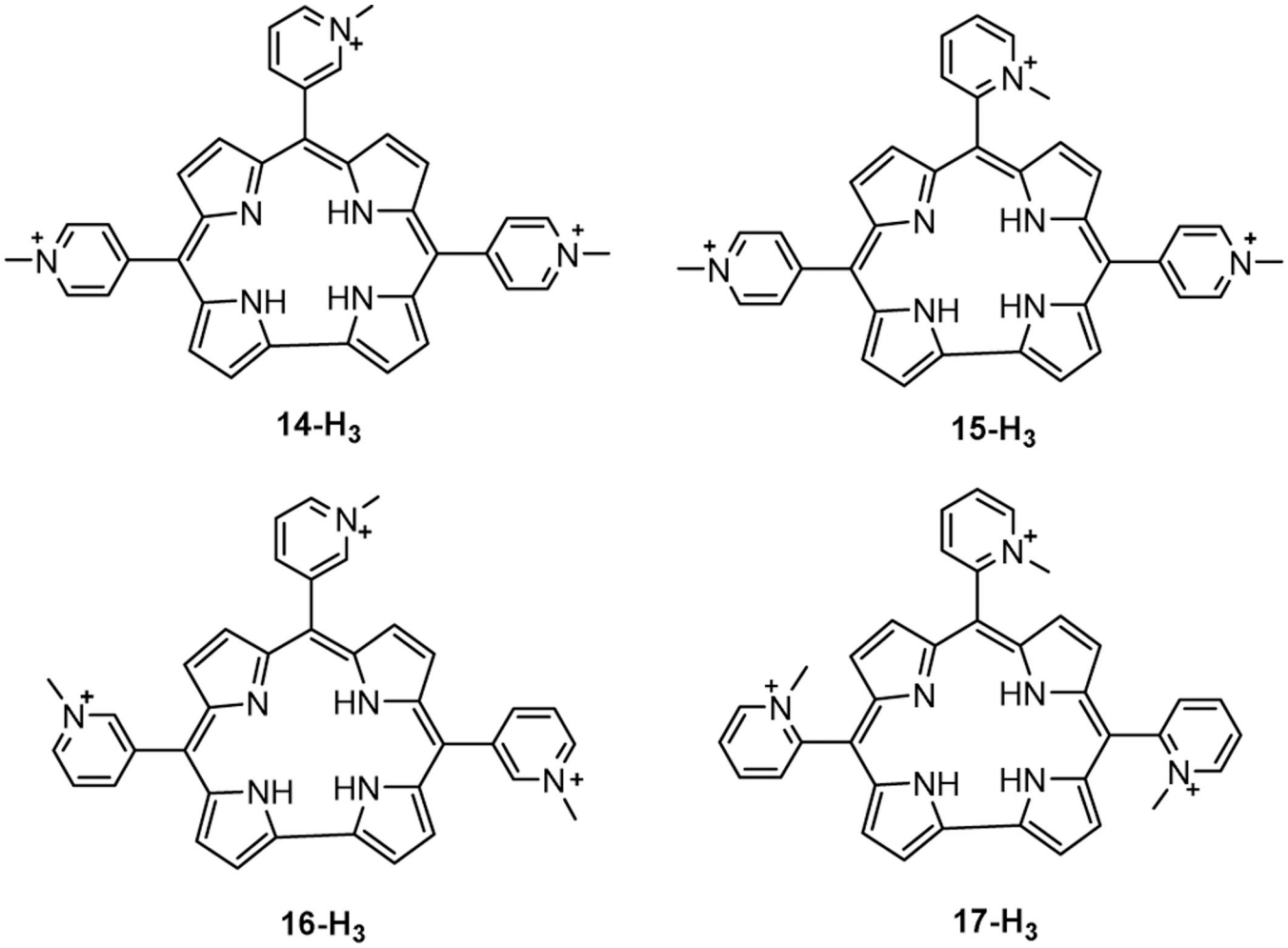

Chart 5.
Structures of free-base isomers **14**-H_3, **15**-H_3, **16**-H_3, and **17**-H_3.

Table 1.

Comparison of IC_{50} cytotoxicity values of **1**-Au, **1**-Ga and cisplatin in human cancer cell lines. Reproduced from ref. 64. Copyright 2014 The Royal Society of Chemistry.

Cell line		**DU145**	**SK-MEL-28**	**MDA-MB-231**	**OVCAR-3**
Tumor type		prostate	Melanoma	breast	ovarian
IC_{50} (μM)	**1-Au**	47.9	26.8	19.7	27.5
	1-Ga	158.9	131.4	129.2	274.2
	cisplatin	81.0	36.8	44.8	22.8

Table 2.

IC_{50} cytostaticity values for **1**-Au and **1**-Ga. Reproduced from ref. 64. Copyright 2014 The Royal Society of Chemistry.

Cell line		DU145	SK-MEL-28	MDA-MB-231	OVCAR-3
IC_{50} (μM)	1-Au	68.5	35.6	75.1	25.4
	1-Ga	>350.0	201.9	322.5	>350.0

Table 3.

Comparison of IC_{50} cytotoxicity values of **1**-Ga, Ga(ACtpfc) and Ga(3-ctpfc) in human cancer cell lines. Reproduced from ref. 114. Copyright 2016 National Academy of Sciences.

Cell line		**DU145**	**SK-MEL-28**	**MDA-MB-231**	**OVCAR-3**
Tumor type		prostate	Melanoma	breast	ovarian
IC_{50} (μM)	**1-Ga**	158.9	131.4	129.2	274.2
	Ga(ACtpfc)	17.6	14.4	13.7	12.7
	Ga(3-ctpfc)	12.9	4.8	15.3	11.1